Technical Report JSR 74-7

February 1976

LOW-ANGLE RADAR TRACKING

By: A. M. PETERSON, J. F. VESECKY, A. M. DESPAIN, F. W. PERKINS, R. A. MULLER

Contract No. DAHC15-73-C-0370
ARPA Order No. 2504
Program Code No. 3K10
Date of Contract: 2 April 1973
Contract Expiration Date: 30 June 1976
Amount of Contract: $2,062,014

Sponsored by

DEFENSE ADVANCED RESEARCH PROJECTS AGENCY
ARPA ORDER NO. 2504

DISCLAIMER NOTICE

THIS DOCUMENT IS THE BEST QUALITY AVAILABLE.

COPY FURNISHED CONTAINED A SIGNIFICANT NUMBER OF PAGES WHICH DO NOT REPRODUCE LEGIBLY.

UNCLASSIFIED

SECURITY CLASSIFICATION OF THIS PAGE (When Data Entered)

REPORT DOCUMENTATION PAGE

READ INSTRUCTIONS BEFORE COMPLETING FORM

(14) 1. REPORT NUMBER: SRI-JSR-74-7

2. GOVT ACCESSION NO.

3. RECIPIENT'S CATALOG NUMBER

4. TITLE (and Subtitle)

(6) LOW-ANGLE RADAR TRACKING

5. TYPE OF REPORT & PERIOD COVERED

(9) Technical Report

6. PERFORMING ORG. REPORT NUMBER

(16) SRI Project 3000

7. AUTHOR(s)

(10) A. M. Peterson, J. F. Vesecky, A. M. Despain, F. W. Perkins, R. A. Muller

8. CONTRACT OR GRANT NUMBER(s)

(15) Contract DAHC15-73-C-0370, ARPA Order-2504

9. PERFORMING ORGANIZATION NAME AND ADDRESS

Stanford Research Institute
Menlo Park, California 94025

10. PROGRAM ELEMENT, PROJECT, TASK AREA & WORK UNIT NUMBERS

11. CONTROLLING OFFICE NAME AND ADDRESS

Defense Advanced Research Projects Agency
1400 Wilson Boulevard
Arlington, Virginia 22209

(11) 12. REPORT DATE: February 1976

13. NO. OF PAGES: 122

15. SECURITY CLASS. (of this report): UNCLASSIFIED

(12) 115p.

14 MONITORING AGENCY NAME & ADDRESS (if diff. from Controlling Office)

15e. DECLASSIFICATION/DOWNGRADING SCHEDULE

16. DISTRIBUTION STATEMENT (of this report)

Approved for public release; distribution unlimited.

17. DISTRIBUTION STATEMENT (of the abstract entered in Block 20, if different from report)

18. SUPPLEMENTARY NOTES

19. KEY WORDS (Continue on reverse side if necessary and identify by block number)

Low-angle radar tracking
Electromagnetic wave scattering
Radar multipath interference
Radar
Radar systems

20. ABSTRACT (Continue on reverse side if necessary and identify by block number)

A review of the problem of tracking low-elevation-angle radar targets is presented. Central to this problem is the scattering of the target return signals from the surrounding land or water surface. Thus the present state of electromagnetic-wave scattering theory is reviewed as it applies to this problem. Scattering at low grazing angles is given special attention, and some relevant lunar bistatic radar data are compared with current theory. Various radar system design considerations and possibilities for improving current systems are considered. It is concluded that both scattering theory and experimental measurements of radar signal scattering should be further developed. It is apparent that a very large variety of techniques can be used to improve low-angle tracking capability in the future and even in current systems. It is also clear that in the future, radar systems could have considerably improved low-angle tracking ability.

DD FORM 1 JAN 73 1473

EDITION OF 1 NOV 65 IS OBSOLETE

UNCLASSIFIED

SECURITY CLASSIFICATION OF THIS PAGE (When Date Entered)

332500

4/B

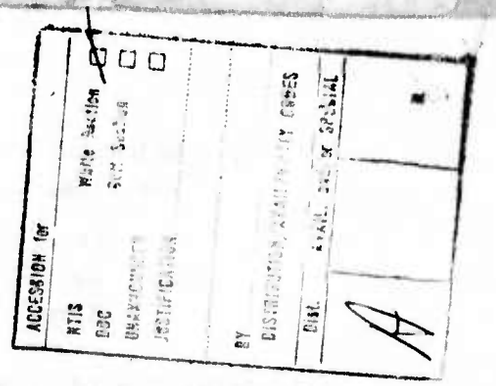

CONTENTS

ILLUSTRATIONS

TABLES

ACKNOWLEDGMENTS

This work was primarily accomplished during the 1974 JASON Summer Study. W. D. White, of AIL, G. L. Tyler of Stanford University, J. H. Cunningham of GRC, J. Welch of the USAF, and R. Barnes of SRI all participated in the summer study discussions and their contributions were not only very important but also greatly appreciated by the authors. All the support furnished by the staff of SRI, directed by R. S. Leonard, was very instrumental in this work. Especially appreciated were the efforts of E. Patrick, L. Benesi, A. Lopker, and D. Williams in the various phases of the work, and a careful reading of the manuscript by R. Tsunoda. The efforts of C. B. Vesecky in translating some of the Russian book by Bass and Fuchs were especially instrumental in the work on scattering theory.

I INTRODUCTION

A. The Low-Angle Tracking Problem

Radar targets at long range and low altitude are very difficult to detect and are especially difficult to track. This is because the radiation scattered by the target is reflected by the ground to the radar antenna and, as a result, in the simplest case the direct return is mixed with a coherent scattered return (see Figure 1). This scattered signal adds constructively or destructively, depending on the exact geometrical relationships between the target, ground, and radar antenna. When this process occurs at very low radar beam elevation angles, the scattered signal falls within the main antenna beam. In effect, the scattered signal is a multipath return from the target that causes an "image" of the target to appear below the horizon. Thus many monopulse radar systems will, when tracking a low-angle target, center on the horizon or become somewhat unstable, depending on the exact phase relationship of the multipath and direct radar return signals. At times, monopulse radars will even track the subterranean image of the target.

Techniques to improve low-angle tracking capability have been the subject of increasing interest as general radar performance has improved. It is increasingly important to know the limits of performance possible in ground-controlled-approach and enroute air surveillance radar systems as the air traffic around airports increases and the danger of air collisions increases.

Some very expensive weapon systems are built around certain assumptions concerning the low-angle tracking ability of installed defensive

radar systems. The payoffs for gaining a better understanding of low-angle tracking are further examined by Smith and Melling (1974). Barton (1974) has recently reviewed the low-angle tracking problem.

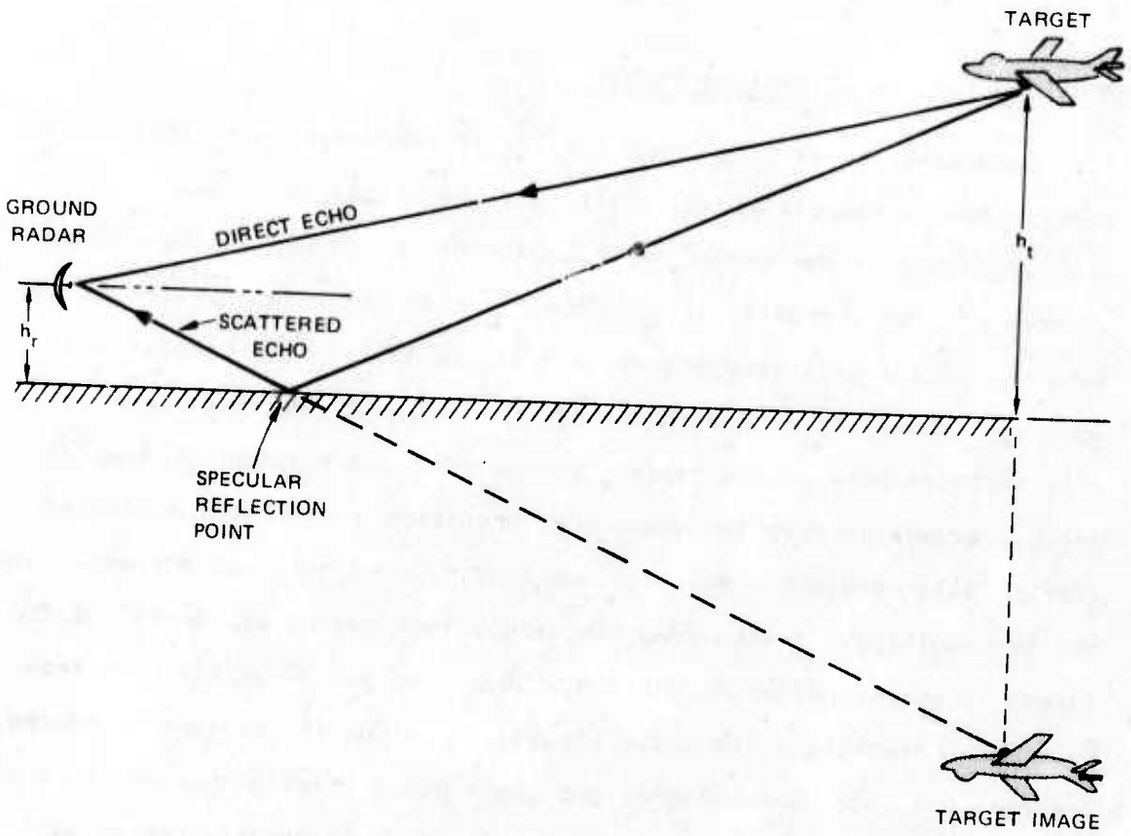

FIGURE 1 ILLUSTRATION OF THE MULTIPATH PROBLEM FOR SPECULAR REFLECTION FROM A FLAT EARTH

B. Electromagnetic Wave Scattering

A key issue in low-angle multipath propagation is the scattering process. At very low grazing angles, the scattering process is much more complex than at near normal incidence. Shadowing, multiple reflections, surface roughness, and earth curvature effects all become important considerations at grazing incidence.

Because of these difficulties, very little scattering theory is applicable to these low angles. Meaningful experiments in these low-

angle regimes are also very difficult to perform. The result is that there is only a little information available that concerns the single most important feature of the low-angle tracking problem. Section II of this report briefly reviews the present state of knowledge of low-angle scattering processes and compares some relevant lunar bistatic radar data with theory.

C. Radar Systems for Low-Angle Tracking

Recently several radar techniques have been proposed to improve low-angle tracking capability. The most impressive work demonstrated to date is that of White (1974). His method involves complex signal processing of the radar return as received from several horns of a dish antenna or in conjunction with an array antenna. Dax (1973) proposed a similar approach. Sherman (1966, 1971), Peebles and Berkowitz (1968), Peebles (1971), Peebles and Goldman (1971), Howard et al. (1971, 1973), and Symonds and Smith (1973) all proposed and reported on the use of complex-angle signal processing of the radar returns for low-angle and multiple-target radar systems. Other signal-processing approaches have been suggested by Von Schlachta (1973), Sklar and Schweppe (1964), Pollon (1967), Pollon and Lank (1968), and Ksienski and McGhee (1968). These are more general clutter and multiple-target studies but are applicable to the low-angle tracking problems. These and some additional possibilities for improving low-angle tracking capability are considered in Section III.

Section III also considers several possibilities for rejecting the reflected radar return by the use of advanced antenna techniques, terrain modification, selective siting, and radar fences.

Conclusions and recommendations are presented in Section IV.

II ELECTROMAGNETIC WAVE SCATTERING--APPLICATIONS TO LOW-ANGLE TRACKING

A. General

The analysis of electromagnetic wave scattering from rough surfaces has become increasingly important with the advance of radar technology since World War II. Theoretical work has tended to be separated into two groups: (1) the traditional radar community with interests in predicting the statistical properties of the scattered signal when the surface properties are fairly well known (e.g., the radar clutter problem), and (2) the astronomical and geophysical community where one wants to obtain statistical information on an unknown surface from a knowledge of the scattered field (e.g., radar astronomy of planetary surfaces and remote sensing of the terrestrial environment). Information from both these communities should be sought in attacking a particular problem. Some useful general and review sources are Barrick and Peake (1967), Barrick (1970), Bass and Fuchs (1972), Beckmann and Spizzichino (1963), Evans (1970), Evans and Hagfors (1968), Simpson (1973), Skolnik (1970, Chapters 22, 25, and 26), and Tyler and Ingalls (1971).

This section will review some necessary general scattering theory, but will concentrate on those features relevant to the problem of low-angle radar tracking. The magnitude and statistical nature of the scattered component at the radar will be the main item of interest. Several questions arise. For example, will the scattered component phase be coherent or incoherent with respect to the direct return, and on what time scale will any phase coherence persist? How much will the scattered return be Doppler-shifted with respect to the direct return? The treatment below will certainly

be far from complete. Our aim is simply to report the features of scattering theory that seemed most relevant during the 1974 JASON summer study.

B. Rough-Surface Scattering Theory

1. Brief Overview of Scattering from Rough Surfaces

The basic scattering geometry is illustrated in Figure 2. A signal is transmitted along $\vec{r}$ toward a target, T. It is scattered by the target and returns to the radar receiver via the direct path, TR, and via a number of scatter paths such as TOR. The resultant E field at R is then the vector sum of the wave E fields arriving via the various return paths.

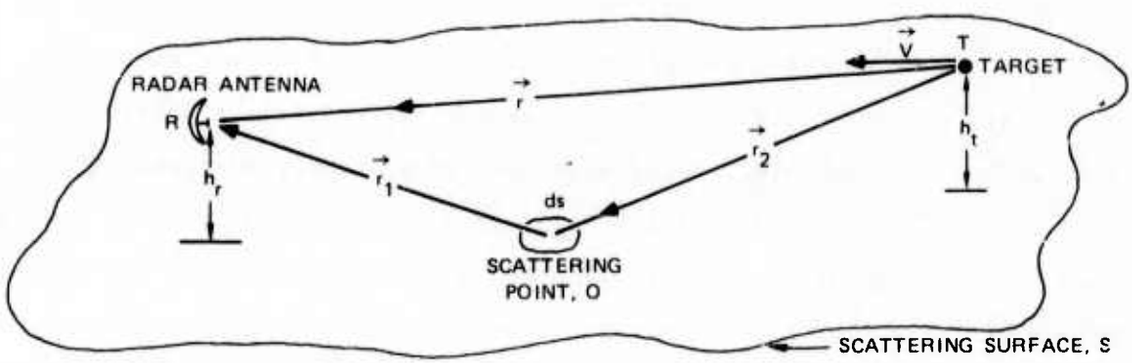

FIGURE 2 SCATTERING GEOMETRY. A radar pulse transmitted from the radar site, R, is scattered by the target, T, and returns to the radar via the direct path, TR, and a collection of paths involving a scattering from the Earth's surface such as the path, TOR. The heights off the mean surface of the radar and target are h_r and h_t, ds is an elemental scattering area, and $\vec{v}$ is the target velocity vector.

Consider a radar receiver that transmits and receives a horizontally polarized wave. As a simplification we will consider only the single component of the electric field parallel to the surface S and perpendicular to $\vec{r}$. This is not unreasonable, since waves arriving at R will be confined by the antenna to directions very nearly along $\vec{r}$. Other electric-field components can of course be considered separately. Let the E field arriving at the target be

$$\frac{E_{TR} e^{ikr}}{r} .$$

The direct-echo E field then becomes

$$E_{RD} = \frac{E_{TR} e^{ik2r} \rho_T e^{i\psi_T}}{r^2} \tag{1}$$

where $\rho_T e^{i\psi_T}$ is the reflection coefficient of the target and the factor $e^{i\omega t}$ has been supressed to simplify the mathematical expressions.

To calculate the electric field E_{RS} arriving at the receiver via surface scatter paths, we will use the Helmholtz integral of physical optics. At each point, O, of the scattering surface, S. we will calculate the scattered electric field by assuming the existence of a reflecting plane tangent to the surface at the point O. Following an approach similar to the work of Beckmann and Spizzichino (1963, pp. 17-22 and 178-181) we have

$$E_{RS} = \frac{-iE_{TR}\left(\rho_T e^{i\psi_T}\right) e^{ikr}}{2\lambda r} \iint_S \frac{g_R e^{ik(r_1+r_2)}}{r_1 r_2}$$

$$\cdot \left\{ \left[(1+R) \frac{\vec{r}_1 \cdot \hat{n}}{r_1} \right] + \left[(1-R) \frac{\vec{r}_2 \cdot \hat{n}}{r_2} \right] \right\} ds \tag{2}$$

where $R = \rho_s e^{i\psi_s}$ is the Fresnel reflection coefficient for the reflecting plane at O, $\hat{n}$ is a unit vector normal to the local surface at point O, and g_R is the voltage gain of the receiving antenna along $\vec{r}_1$. This particular formulation of electromagnetic wave scattering from a rough surface is

usually called quasispecular scattering. Since the surface may be rough, $\hat{n}$ is not necessarily perpendicular to the mean surface. In fact, the roughness of the surface is modeled by letting the direction of the local normal, $\hat{n}$, vary in a random manner about a mean value.

Though there are alternative formulations, Eq. (2) is especially useful since it clearly shows the actual physical summation process as well as other important general features. If the surface S is relatively homogeneous and smooth, $\hat{n}$ will be very nearly perpendicular to the mean surface and the exponential term $e^{ik(r_1+r_2)}$ will tend to dominate the behavior of the integral. The received wave will thus be mainly coherent and similar to that expected from the specular-reflection case described below. If the surface S is comparatively rough and/or highly nonhomogeneous, varying randomly from one scattering point to another, the exponential term will not be important and the received wave will tend to be incoherent. Waves scattered from rough surfaces in nature will in general have both coherent and incoherent components. It is the coherent component that is the most devastating to radars tracking low-elevation targets, because it can add in antiphase to the direct radar echo and cancel the desired signal completely.

When the surface is homogeneous, but still comparatively rough, the geometric factor $(1/r_1 r_2)$ comes into play. This factor tends to divide any incoherently scattered return into <u>foreground</u> (r_1, small) and <u>horizon</u> (r_2, small) components over regions where g_R is not a strong function of the location of the scattering point. Barton (1974, p. 691) and Beckmann and Spizzichino (1963, Chapter 2) give examples of specific cases.

Scattering from a rough surface is best understood by first considering a perfectly smooth, homogeneous, infinite flat surface. Reflection from such a surface is governed by Snell's law ($\theta_i = \theta_s$, $\varphi_s = 0$ in Figure 3)

and the classical Fresnel reflection coefficients given in Eqs. (22) and (23) below. Such a reflection ($\theta_i = \theta_s$, $\varphi_s = 0$) is called <u>specular</u> and the term reflection is used since no power is scattered in other directions. Specular reflection is <u>coherent</u> in that the reflected field parameters (amplitude and phase) are uniquely predictable--i.e., deterministic, as shown below. Any real surface is, of course, finite, so some energy is scattered into other directions close to the specular direction ($\theta_s = \theta_i$, $\varphi_s = 0$), but for the large reflecting areas considered here the specular component will dominate strongly.

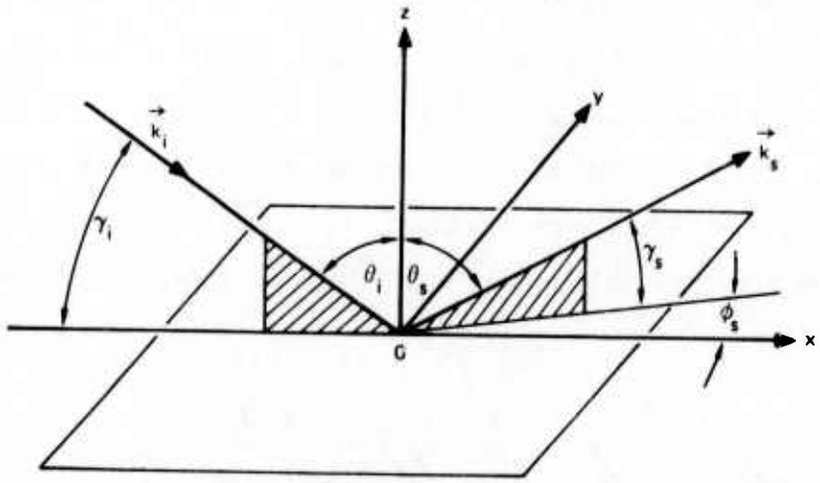

FIGURE 3 LOCAL FRAME OF REFERENCE FOR AN APPROXIMATELY FLAT SCATTERING SURFACE. The angle of incidence, θ, grazing angle, γ, and wave vector ($\vec{k}$, $|\vec{k}| = 2\pi/\lambda$) for the incident wave are denoted by the subscript i, while the subscript s identifies the scattered-wave parameters.

In considering a rough surface, we have several types of surface models from which to choose: <u>semi-empirical models</u>, which are based on simple physical ideas and matched to given sets of data by parameter adjustments; <u>geometric models</u> in which simple geometric shapes are arranged randomly on a plane; and <u>statistical models</u> in which the surface height above the reference (x,y) plane is a random variable. The statistical approach is the most general and we shall consider such models for the

most part. However, a number of problems--e.g., diffuse scattering--have not been satisfactorily solved via the statistical approach and one must use an alternative model. Barrick (1970) reviews results from all three approaches with an emphasis on backscatter.

In the statistical approach the surface is characterized by an average (rms) height deviation, h, from the x,y plane and a correlation length ℓ. As h increases from zero, less power is reflected specularly and more power is scattered into nonspecular directions. A useful parameter is defined by $g = kh\ (\sin \gamma_i + \sin \gamma_s)$, where $k = 2\pi/\lambda$. For a slightly rough surface ($g \ll 1$), the coherent, specular component will still be present; but an incoherent component will become increasingly important as g increases, especially in directions away from the specular direction. For $g \gtrsim 1$ the surface is rough enough that the incoherent component dominates. Figure 4 illustrates the transition from smooth to rough. See Beckmann and Spizzichino (1963, Chapter 5) for more details.

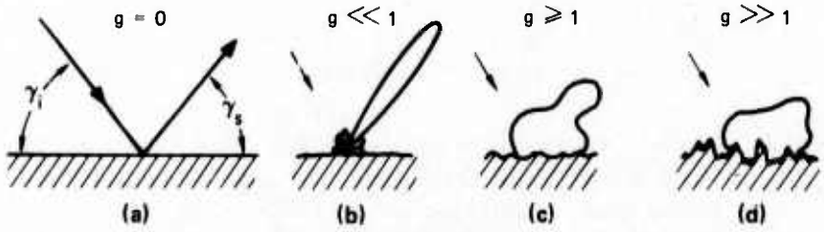

FIGURE 4 TRANSITION FROM SPECULAR REFLECTION TO DIFFUSE SCATTERING. The surfaces vary from a smooth surface with $g = 0$ in (a) to a very rough surface with $g \gg 1$ in (d). The parameter g is defined as $(2\pi h/\lambda)(\sin \gamma_i + \sin \gamma_s)$, where h is the rms surface height deviation and λ is the wavelength (after Beckmann and Spizzichino, 1963, p. 90).

2. Specular Reflection

We define the field (as opposed to power) reflection coefficient as Beckmann and Spizzichino (1963, p. 22) define it: $\rho = E_R/E_{RO}$, where E_R is the received field and E_{RO} is the field that would be reflected specularly ($\gamma = \gamma_i = \gamma_s$) by a smooth, perfectly conducting plane under the same circumstances. For a perfectly smooth dielectric surface, $\rho = \rho_o e^{j\alpha_o}$, where $\rho_o e^{j\alpha_o}$ is given by Ramo et al. (1966, p. 358). For a slightly rough surface we let $\rho_o \rightarrow \rho_o \rho_{spec}$ [cf. Beckmann and Spizzichino (1963, p. 80-93)], where $\langle \rho_{spec} \rangle$ is the average value of ρ_{spec}.

$$\langle \rho_{spec} \rangle = \exp\left[-\frac{1}{2}\left(\frac{4\pi h \sin\gamma}{\lambda}\right)^2 \right] \tag{3}$$

One might conclude from this formula that for γ sufficiently small, a surface will appear smooth ($\langle \rho_{spec} \rangle \rightarrow 1$) regardless of the roughness. That is, the Rayleigh criterion for a smooth surface holds for arbitrary h. We shall see below that since shadowing effects have thus far been neglected, Eq. (3) will not generally hold for any $h > 0$ because shadowing of one part of a random rough surface by another tends to reduce ρ as $\gamma \rightarrow 0$.

3. Quasispecular Scattering Theory

This statistical model postulates a gently undulating random surface where the radius of curvature is everywhere much greater than λ. The analysis assumes that all of the scattering from such a rough surface comes from "specular points" that are locally aligned such that they reflect signals specularly to the receiver. This model, sometimes known as the cracked-egg model (boiled egg), is analogous to moonlight reflecting off a slightly rough sea. For a Gaussian distribution of surface

heights and a Gaussian autocorrelation function, the bistatic radar cross section becomes (Tyler and Ingalls, 1971)

$$\sigma^o(\theta_i, \theta_s, \phi_s) = \frac{q^4 \cot^2 \beta_o}{2 q_z^4} \exp\left(\frac{-\tan^2\beta}{2\tan^2\beta_o}\right) |R(\gamma, \varepsilon)|^2 \qquad (4)$$

where $\vec{q} = (\vec{k}_i - \vec{k}_s)/k$; $\vec{k}_i$ and $\vec{k}_s$ are the incident and scattered wave vectors in Figure 3 and $k = 2\pi/\lambda$; $\tan^2\beta_o$ is the mean square unidirectional slope $= (h/\ell)^2$; h is the rms height; ℓ is the correlation length; and $\tan^2\beta = q_{||}^2/q_z^2$, where $q_{||}$ and q_z are the components of $\vec{q}$ parallel and perpendicular to the mean surface at the point of incidence. $|R(\gamma,\varepsilon)|$ is the Fresnel reflection coefficient for specular reflection from a perfectly smooth dielectric surface (see Barrick, 1970, p. 700). For a perfectly conducting, smooth surface, $|R(\gamma,\varepsilon)| \to 1$. The scattered signal predicted by this model has both coherent and noncoherent components, with the noncoherent component dominating as g increases (see Beckmann and Spizzichino, 1963, Chapter 5 and Figure 4 above).

Quasispecular theory has been developed over a number of years, by Beckmann and Spizzichino (1963), who refer to quasispecular as diffuse scattering, and by others, with a number of variations--e.g., non-Gaussian statistics. A large variety of lunar and terrestrial radar data are in reasonably good agreement with quasispecular theory as shown by Barrick (1970, pp. 753). However, quasispecular theory breaks down at low grazing angles unless shadowing, and possibly other effects, are included. A comparison of quasispecular theory including shadowing with relevant lunar bistatic data is made later in this section. For certain geometries and surfaces a "diffuse component" due to small-scale roughness may dominate the quasispecular component, as discussed below.

4. Shadowing Theory

At small grazing angles the shadowing of one part of a surface by another and multiple reflections between surface elements become increasingly important for both geometrical and statistical type scattering models. In the case of statistical models, the multiple-scattering problem has not yet been attacked quantitatively, but considerable efforts have been made on the shadowing problem--e.g., Beckmann (1965), Brockleman and Hagfors (1966), Smith (1967), and Bass and Fuchs (1972, in Russian).

The chapters on shadowing in Bass and Fuchs (1972) have recently been translated by C.B. Vesecky, but are not generally available in English; so a brief comment on them is appropriate. They begin with a general formulation that includes both shadowing and multiple scattering, but specializes to single scattering. They characterize the relevant properties of a random surface with normally distributed height and slope by a function Λ as follows:

$$\Lambda(a) = \frac{1}{2a}\left[\sqrt{\frac{2}{\pi}}\, e^{-\frac{a^2}{2}} - a\,\mathrm{Erfc}\left(\frac{a}{\sqrt{2}}\right)\right] \tag{5}$$

where

$$a = \tan\gamma_i / \left(\sqrt{2}\,\tan\beta_o\right) \quad , \quad \mathrm{Erfc}\,(X) = 1 - \frac{2}{\sqrt{\pi}}\int_0^X e^{-t^2}\,dt \tag{6}$$

and $\tan\beta_o$ is the unidirectional rms surface slope for a Gaussian surface. The function Λ is also defined for the variable $b = \tan\gamma_s / \left(\sqrt{2}\,\tan\beta_o\right)$.

Bass and Fuchs develop a reflection coefficient $\langle \rho_{spec} \rangle$ for the average reflected field in the limiting case of weak shadowing ($a \gg 1$) and near-specular reflection

$$\langle \rho_{spec} \rangle = \left[1 - \text{Erfc}\left(\frac{a}{\sqrt{2}}\right)\right] \quad [1 - 2\Lambda(a)]\, e^{-2(kh \sin \gamma_i)^2} \quad . \qquad (7)$$

Note that Eq. (7) is simply Eq. (3) with a multiplicative correction factor to account for shadowing. In the limiting case of strong shadowing ($a \ll 1$), $\langle \rho_{spec} \rangle$ becomes

$$\langle \rho_{spec} \rangle = \left[1 - \text{Erfc}\left(\frac{a}{\sqrt{2}}\right)\right] \frac{1}{\sqrt{2\pi}}$$

$$\int_{-\infty}^{\infty} \exp\left[-\frac{x^2}{2} + iq_z hx - \Lambda(a)\text{Erfc}(x)\right] dx \quad . \qquad (8)$$

They also derive results for the average power reflection coefficient by calculating a function $Q(\gamma_i, \gamma_s)$ such that the reflected power with shadowing included is just Q times the power reflected without shadowing. In the case of strong shadowing ($a \ll 1$) we have for forward scatter:

$$Q(\gamma_i, \gamma_s) = \frac{1 - \exp\{-[\Lambda(a) + \Lambda(b)]\}}{\Lambda(a) + \Lambda(b)} \qquad (9)$$

and for backward scatter:

$$Q(\gamma_i, \gamma_s) = \frac{1 - e^{-\Lambda(c)}}{\Lambda(c)} \tag{10}$$

where c is the minimum of a and b.

Following these results, Bass and Fuchs examine the case where $a \approx 1$, and they derive effective distribution functions for the height and slope based on the work of Smith (1967). A new shadowing function $\tilde{Q}$ is derived for forward scatter:

$$\tilde{Q}(\gamma_i, \gamma_s) = \frac{1}{1 + \Lambda(a) + \Lambda(b)} \tag{11}$$

and for monostatic backscatter:

$$\tilde{Q}(\gamma_i) = \frac{1}{1 + \Lambda(a)} \quad . \tag{12}$$

The backscatter result, Eq. (12), is in agreement with Smith (1967). A comparison of the effective probability distributions associated with Q and $\tilde{Q}$ and the simulation experiment of Brockleman and Hagfors (1966) favors the choice of $\tilde{Q}$. However, the choice does not seem to be critical for the cases compared. Clearly, this Soviet effort on the shadowing problem is substantial, and the authors are fully aware of published Western results. However, the final results are essentially the same as those of Smith (1967) in the case of intermediate ($a \approx 1$) and strong ($a \ll 1$) shadowing. The fact that they do not compare their theory with Soviet experiments probably indicates that such experiments do not exist as far as the open Soviet literature is concerned.

Needless to say, shadowing is extremely important for low-angle radar tracking. Later in this section we compare this shadowing theory with forward-scatter data collected during an Apollo 16 bistatic radar experiment that explored the lunar surface. We will see that for grazing angles (γ_i and γ_s) smaller than or comparable to the rms surface slope (i.e., $a \leq 1$) scattering by the quasispecular process is significantly reduced by shadowing. This is especially important because one would expect an increase in the bistatic radar cross section as γ_i and γ_s approach zero, on the basis of quasispecular theory for a plane surface without shadowing. For a sufficiently curved surface, the divergence factor, D, reduces the scattered power seen by an observer at low grazing angles--see Section II-C below.

5. Diffuse-Scattering Theory

The quasispecular scattering from a rough surface described above applies to scattering angles near the specular direction ($\theta_s \approx \theta_i$). In addition, there is usually a diffuse scattering process due to roughness on a scale $\leq \lambda$, a scale much smaller than the roughness giving rise to the quasispecular component. This diffuse component will generally dominate the quasispecular component for scattering angles far enough away from the specular direction. At present there is no widely accepted statistical type analysis of this diffuse component and one is forced to fall back on a semi-empirical model such as the generalized Lambertian law

$$\sigma^o = K_1(\cos\theta_i \cos\theta_s)^{n_1} \tag{13}$$

or the Lommel-Seeliger law

$$\sigma^o = K_2\left(\frac{2 \cos \theta_i \cos \theta_s}{\cos \theta_i + \cos \theta_s}\right) \quad . \tag{14}$$

K_1, n_1 and K_2 are free parameters adjusted to fit a given experimental data set. Barrick (1970, p. 677) comments that these two laws compare favorably with some backscatter data in directions where diffuse scattering is thought to dominate. At low grazing angles, Barton (1974, p. 690) uses what is equivalent to the Lambertian law with $K_1 = 4\pi(h/\beta_o\lambda)^2$ and $n_1 = 1$ in his analysis of diffuse scattering in the low-angle radar tracking problem.

6. Scattering from Vegetation

As one can well imagine, vegetation is difficult to model as a radio-wave scatterer. A successful model must account for several general characteristics observed experimentally, as follows. The incident wave is attenuated as it propagates into the vegetation layer so that the depth of the layer is not important so long as it is greater than λ (Peake, 1959a). (This implies that a vegetation layer does not have to be very thick to effectively mask the underlying terrain.) The scattering properties must also depend on the dielectric properties, moisture content, size, and density of the vegetation. Since vegetation is often of a linear form (e.g., grass, pine needles, etc.), one expects some significant dependence of the return on the polarization of the incident wave.

Barrick (1970, p. 689) reviews a model by Peake (1959a and 1959b) in which vegetation is modeled by a collection of thin dielectric rods, randomly arranged, but preferring the vertical, and terminated on the

upper end by a flat horizontal plane. The model falls in the geometric class of models and is, according to Barrick, the only model that can qualitatively and quantitatively describe scattering from vegetation-covered surfaces. As with the quasispecular theory above, it does not take account of shadowing and multiple scattering and so is likely to fail at the small grazing angles (γ in Figure 3) that are of interest in the low-angle radar tracking problem.

7. Components of the Resultant E Field at the Radar Receiver

Let us think of the electric-field vector at the receiver R in Figure 2 as the sum of three components: The E field ($\vec{E}_T$) backscattered from the target along TR, the E field ($\vec{E}_R$) coherently reflected at the specular reflection point (where $\theta_s = \theta_i$), and the scattered E field ($\vec{E}_s$) which is incoherent. At a given instant in time the resultant $\vec{E}$ would appear somewhat as in Figure 5, depending on the relative magnitudes of the three components. We will assume here that all three components are received with approximately the same antenna gain as in the case of low-angle radar tracking. If the surface is only slightly rough, specular reflection dominates, $E_s \sim 0$, $E_R \sim E_T$, and the resultant E varies between about 0 and 2 E_T according to the path difference between r and $r_1 + r_2$ in Figure 2. Now if, in this case, the target T moves, E varies systematically from ~ 0 to $\sim 2\ E_T$ according to the changes in path difference, with disastrous results if a monopulse tracking radar is used (see Hey and Parsons, 1955, and Evans, 1966). For the rough surface case, $E_R \sim 0$, $E_T > E_s$, and E varies between $E_T + E_s$ and $E_T - E_s$. In this case $\vec{E} = \vec{E}_T + \vec{E}_s$, and as the target moves (or the sea surface changes) $\vec{E}_s$ varies in a random manner, but with a certain autocorrelation time, τ_s -- i.e., a characteristic time during which the scattering surface changes from one realization of an ensemble of random surfaces to another, and

hence during which $\vec{E}_s$ changes significantly. Beckmann and Spizzichino (1963) consider the rough-surface case (p. 120) and estimate (p. 282) a horizontal autocorrelation distance $\Delta' x$ that we can convert to an autocorrelation time τ_s by dividing by the target's velocity (V):

$$\tau_s = \frac{\Delta' x}{V} \approx \frac{2\lambda r^2}{Vh^2} \tag{15}$$

where h is the greater of the two heights h_r and h_t in Figure 2. The period of the variation τ_R in the slightly rough (specular reflection) case (p. 283) is similarly

$$\tau_R = \frac{\Delta x_s}{V} \approx \frac{r^2 \lambda}{2\, V h_r h_t} \tag{16}$$

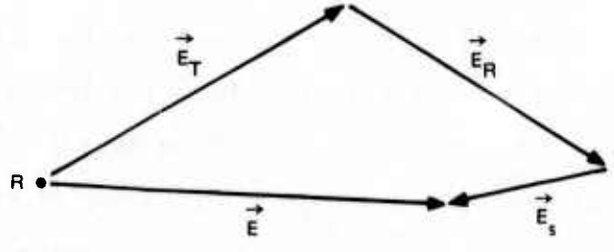

FIGURE 5 COMPOSITION OF THE ELECTRIC-FIELD VECTOR AS SEEN AT THE RADAR, R, IN FIG. 2. The electric field at the radar, $\vec{E}$, is the sum of the direct wave, $\vec{E}_T$, from the target, the reflected or coherently scattered wave, $\vec{E}_R$, and the incoherently scattered wave, $\vec{E}_s$.

Consider the case of a target in level flight over land where h_t = 100 m, h_r = 5 m, V = 250 m s^{-1} (560 mph), r = 20 km and λ = 3 cm (X-band). Thus, from Eqs. (15) and (16) we have $\tau_s \sim 10$ s and $\tau_R \sim 48$ s. If we accept Eqs. (15) and (16) as correct, E_s varies extremely slowly

on the time scale of a typical radar pulse repetition period ($\approx 10^{-3}$ s). In fact, for times small compared to τ_s, specularly reflected (E_R) and scattered (E_s) components look virtually the same to the radar receiver except for magnitude. Beckmann and Spizzichino (1963, p. 284) point out that τ_s may be shorter than given by Eq. (3) due to atmospheric scintillation effects. Indeed, measurements by Bullington (1954, p. 1259) indicate that τ_s should be about 0.5 s for one particular case.

This analysis would indicate that over land, care must be taken in averaging signals to reduce the errors caused by incoherent scattering. This is because the scattered field at the receiver will not vary appreciably on time scales shorter than τ_s and therefore averaging over times less than τ_s will not be effective in reducing unwanted random signal fluctuations.

8. Doppler Shift of the Direct and Scattered Echoes

The radar echo from a moving target is Doppler-shifted by an amount $\Delta f = f - f_o$ where f is the observed frequency and f_o is the transmitted frequency. Referring to Figure 2, $\Delta f = (f_o/c)\ (\hat{r} \cdot \vec{V} + \hat{d} \cdot \vec{V})$ where c is the velocity of light, $\hat{r}$ is a unit vector along $\vec{r}$, and $\hat{d}$ is a unit vector along the direction with which the echo signal leaves the target. For the direct echo along path TR we have $\hat{d} = \hat{r}$, whereas for the scattered echo via path TOR, $\hat{d} = (\vec{r}_2/|\vec{r}_2|)$. Since Δf will vary with the direction of $\hat{d}$, it is in principle possible to distinguish between the direct and scattered echoes on the basis of Doppler shift.

To appreciate the significance of Doppler shift in the low-angle tracking problem, we will consider the somewhat simplified case illustrated in Figure 6. Here we have assumed a flat earth and will consider only echoes that are scattered in the plane of the figure. In spite of these limitations some interesting features will be evident. Applying the formula for Δf given above to the geometry of Figure 6 we have, for the direct echo along TR,

$$\Delta f = (f_o V/c)(2 \cos \alpha) = (f_o V/c) \left\{ 2 \cos \left[\tan^{-1} \left(\frac{h_t - h_r}{G} \right) \right] \right\} \quad (17)$$

and for the scattered echo along TOR,

$$\Delta f = (f_o V/c)(\cos \alpha + \cos \beta)$$

and

$$\Delta f = (f_o V/c) \left\{ \cos \left[\tan^{-1} \left(\frac{h_t - h_r}{G} \right) \right] + \cos \left[\tan^{-1} \left(\frac{h_t}{G - X_s} \right) \right] \right\} . \quad (18)$$

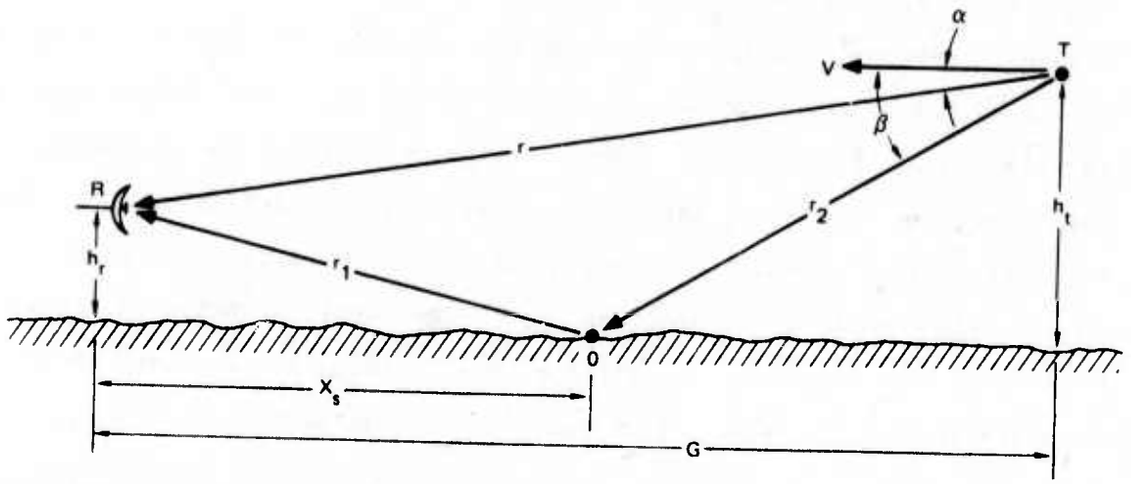

FIGURE 6 GEOMETRY FOR CALCULATING THE DOPPLER SHIFT. The radar echoes arrive at the radar, R, directly from the target, T, via path TR and scattered from the surface—e.g., via the path TOR. G is the ground range from radar to target, and X_s is the ground range to a scattering point, O. The mean surface of the earth is assumed to be flat.

To apply these formulae to a typical low-angle tracking problem, we take a target velocity $V = 250\ ms^{-1}$ (560 mph), a radar wavelength $\lambda = 3$ cm, a radar height $h_r = 5$ m, a target height $h_t = 100$ m, and target ground ranges $G = 10$ and 20 km. In Figure 7 we have plotted the Doppler shift of the scattered echoes as a function of X_s, the ground range of the scattering point, and compared it to the Doppler shift of the direct echo. Considering the curvature of the earth and standard refraction of the radar signal, we see that the real horizon for $h_r = 5$ m is about 9 km. If we consider scattering points above the mean surface, the horizon moves to larger ranges--e.g., for scattering points 1 m above the mean surface the real horizon is about 13 km.

It is clear from Figure 7 that Doppler discrimination between the direct and scattered echoes becomes increasingly difficult as X_s decreases. However, Doppler discrimination could well be useful in discriminating against echoes scattered near the target ($X_s \rightarrow G$). Echoes scattered in this region, known as the "horizon component" of the scattered echo, can in fact be relatively important, as noted in connection with Eq. (2). Such discrimination would be less useful for large values of G (e.g., 20 km), since much of the area near the target would be below the radar's horizon anyway. Only those scattering points lying 7 m and more above the mean surface--e.g., small hills--would be visible at $X_s \approx G = 20$ km.

For both values of G considered here the specular reflection point is very near the radar ($X_s \leq 1$ km), so for a very smooth surface where specular reflection is important, Doppler discrimination would be relatively difficult. As the surface becomes rougher the echo scattered quasispecularly comes from a broader range of values of X_s, some regions being more important than others--cf. Barton (1974, p. 691), and Beckmann and Spizzichino (1963, Chapter 12). Since σ^o for diffuse scattering varies more slowly with position than the factor $(1/r_1 r_2)$ in Eq. (2), the

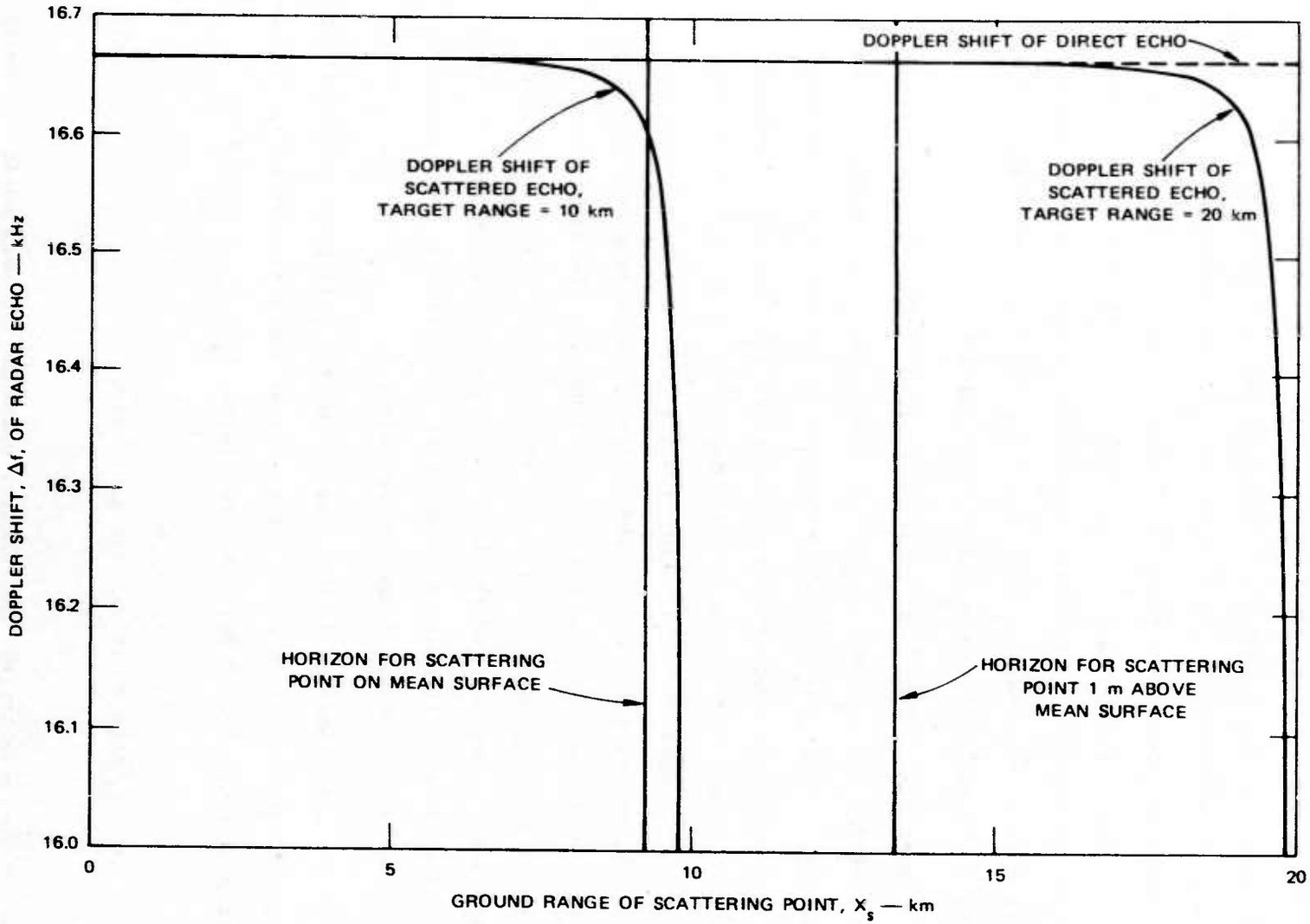

FIGURE 7 DOPPLER SHIFT OF THE DIRECT ECHO AND SCATTERED ECHOES FROM VARIOUS SCATTERING POINTS. Doppler shift is shown as a function of the ground range of the scattering point (X_S in Fig. 6) for targets at 10 and 20 km ranges and 100 m altitude. The radar height is 5 m, λ = 3 cm, and the target velocity is 250 ms^{-1} (560 mph). The geometric horizons for a curved Earth shown above are calculated using standard refraction.

echo arising from a diffuse process will tend to be concentrated near the horizon and near the radar. In general the scattered echo will be composed of a sum of echoes from points with different Doppler shifts, each being weighted according to the size of the bistatic radar cross section σ^o. As mentioned above, the theoretical models for σ^o relevant to the low-angle tracking problem are not at all well established; hence, only qualitative statements are probably justified. However, once adequate low-angle scattering models become available, the Doppler profile (echo intensity vs. frequency) can be easily calculated.

Both Barton (1974, p. 694) and Fjeldbo (1964) have calculated Doppler profiles for specific scattering laws. Barton's calculation uses a scattering law that approaches the Lambertian law [Eq. (13)] for small grazing angles and is specifically addressed to the low-angle tracking problem. He finds the half-power bandwidth Δf to be about 1 Hz or less, depending on the specific case. Only for the case of a very rough surface $(h/\lambda) \gg 20$ and a 105-m-altitude target at 10 km range does he find appreciable scattered echo power more than 2 Hz from the direct target echo. In considering these results one should remember that the correspondence between reality and the Lambertian scattering law used in these calculations is not well known at low angles. However, it is probably as good a choice as any other at the present time.

Fjeldbo (1964) derived a formula for the half-power bandwidth of the scattered-echo spectrum using a statistical model similar to the quasi-specular scattering law of Eq. (4). He assumes $\gamma_i = \gamma_s = \gamma$ and finds

$$\Delta f = 4\sqrt{2 \ln 2} \quad (V_s/\lambda) \tan (\beta_o) \sin \gamma \tag{19}$$

where V_s is the velocity of the specular point on the mean surface. Using the geometry of Figure 6 we find that $V_s = [h_r/(h_r + h_t)]\, V$ where $\vec{V}$ is

assumed parallel to the surface. Using the same parameters as for Figure 7 (i.e., λ = 3 cm, G = 10 km, h_r = 5 m, h_t = 100 m, and V = 250 ms^{-1}), and taking tan β_o = 0.04 (corresponding to moderately rough terrain), we have γ_i = 0.01 rad and Δf = 0.75 Hz. Here again we do not know how realistic Fjeldbo's scattering law is at low angles. Fjeldbo's result has been used in connection with lunar bistatic radar data (Tyler and Simpson, 1970) and predicts reasonable values of the unidirectional rms slope (tan β_o) for γ_i and $\gamma_s \gg \beta_o$. However, at small grazing angles the theory appears to break down, probably because shadowing was neglected (see Tyler and Ingalls, 1971, p. 4775).

Based on these analyses one would have to use very narrowband filters ($\leq$ 1 Hz) to discriminate between direct and scattered echoes by means of Doppler shift. But if, as one might expect from quasispecular scattering theory, the scattered echo for low-angle targets turns out to come from a relatively small number of unshadowed "specular points," each one would have a more or less unique Doppler shift that would change as the target moves. It seems possible that one could exploit this situation by placing the radar at a site such that the Doppler shifts of the dominant "specular points" were as far as possible from the Doppler shift of the target. Alternatively, one might observe the "Doppler tracks" of known "specular points" or even of transponders to obtain information concerning target location. Some really definitive experimental work on scattering at small grazing angles is necessary to evaluate such a possibility. Some suggestions regarding experimental work are given in Section IV below.

9. Deficiencies in Scattering Theory Relevant to Low-Angle Radar Tracking

The outstanding problems in scattering from rough surfaces at low grazing angles are as follows:

(1) Quasispecular scattering theory breaks down at low grazing angles because shadowing and multiple scattering have been neglected. Some theoretical work on shadowing exists, but is untested by experiment (except as done for the lunar surface in Section II-C-4); and multiple scattering is still neglected.

(2) No good statistical or geometric theory exists for the diffuse-scattering component for any grazing angle. To the authors' knowledge, semi-empirical models such as Eqs. (13) and (14) have not been compared with experimental data at low grazing angles.

(3) Scattering from vegetation is clearly a difficult problem, especially at low grazing angles. Peake's model (Barrick, 1970, p. 689) appears to be the only model known that can "describe qualitatively and quantitatively the scattering by vegetation-covered surfaces." But Peake's model deviates from measurements at low grazing angles.

Once scattering laws for a particular range of parameters are well understood from both theoretical and experimental viewpoints, one can predict with confidence how the scattered echo will differ from the direct echo--e.g., in time delay, Doppler shift, intensity, polarization, etc.--and algorithms to do the discrimination can be derived and evaluated. At present the above deficiencies in scattering theory will be reflected as uncertainties in predicted tracking errors for a given radar system.

C. Experimental Data on Microwave Scattering from Reugh Surfaces, and Comparison with Theory

1. General

Experiments gathering data on the scattering of microwave radiation from the Earth's land and sea surfaces have been going on for considerably more than 20 years. In addition, radar waves have been used to explore the Moon's surface and the surfaces of Mars and Venus. This mass of experimental data has encouraged theorists to investigate the problem of electromagnetic-wave scattering from randomly rough surfaces. There have been notable cases of a theory successfully explaining a set of experimental data--e.g., quasispecular scattering theory and lunar radar data. However, when one attempts to compare theory with available experimental data, there are a number of inherent problems.

First, experimental results are often given in terms of the power reflection coefficient (ρ^2) observed under a particular set of experimental conditions. As shown in Section II-C-4 below and in Barton (1974), a theoretical calculation of ρ^2 involves an integration over the scattering surface as well as specialization of the theory to match the experimental conditions. So only one implication of the theory is tested and the point of comparison is an integral quantity. Such a comparison is clearly not an ideal one; yet it is often all that is possible.

Another difficulty arises in the experimental measurement of the scattered wave. A full specification of the scattered wave requires the measurement of the coherency matrix [J] (or the general Stokes parameters) as a function of direction of arrival, time delay, and Doppler shift (see Born and Wolf, 1975, pp. 544-555, and Hagfors, 1967). Experimental measurement of such a full specification is a substantial task and is generally attempted only in radar astronomy experiments such as that by Tyler and Howard (1973) discussed below. Thus the experimental data that

would enable one to make a crucial comparison of theory with experiment are often not available at all or only with substantial data processing.

A genuine test of theory by experiment must include a sufficiently accurate characterization of the scattering surface. For example, the quasi-specular scattering theory developed by Beckmann in Beckmann and Spizzichino (1963) and others requires the unidirectional rms slope of the scattering surface ($\tan \beta_o$) on a scale large compared with the wavelength--say, about 10 λ. A natural surface will also possess roughness on scales shorter than λ as well as on scales very much longer than λ--e.g., hills, etc. At wavelengths in the VHF and UHF ranges even subsurface characteristics can be important. So in a field experiment one must be careful to measure the right parameters over the right scale lengths. Only then can meaningful comparison between theory and experiment be made.

An incisive experiment that will genuinely test a scattering theory must involve a very careful choice of the parameters to be measured, both of the scattered radiation and of the scattering surface. While it would be expensive and probably unnecessary to measure all the conceivable parameters of interest, it should not be beyond the wit of man to design clever experiments that establish the range of parameters over which the critical assumptions of a theory are valid. In fact, a good experiment that establishes the weak points of a particular theory could very well point to the faulty assumptions that need to be rectified in subsequent theoretical developments. In the case of scattering from rough surfaces at very low grazing angles, the critical experiments needed to test current theories have yet to be made, so far as we have been able to determine. Some specific experimental recommendations are made in Section IV.

2. Data on Forward Scattering over Land

It is beyond the scope of this report to survey the literature on the forward scattering of microwaves over land. However, it is useful

to cite some examples of relevant work and to comment on their strong points and weaknesses. One set of experimental data used by Barton (1974) for comparison with theory is that of Bullington (1954). This data set is really a byproduct of the route survey for the transcontinental microwave relay system. Certainly the data are useful, especially since a large number of paths were measured. However, these data cannot be used in a critical test of theory because too many things apparently were not measured. For example, the nature of the scattering surface is recorded only on horizontal scales longer than about 1/2 mile. Bullington in fact concludes that "...the magnitude of the reflection coefficient cannot be predicted accurately from the gross features of the path profile." Of course, these experiments were never designed to test scattering theory and one should be grateful that they were published at all. Even so, they are often quoted in comparisons of theory and experiment.

Barton (1974) quotes reflection-coefficient measurements made by McGavin and Maloney (1959) over dry Colorado range land at about 1 GHz. He then carries out a theoretical calculation that yields power reflection coefficients of 0.16 to 0.25 and compares these to the mean value of 0.12 for the experimental data. This, Barton (1974) concludes, "constitutes good agreement, considering the uncertainties in antenna patterns, surface slopes, masking and illuminating regions." Certainly the theoretical and experimental values are reassuringly close. However, such a comparison of reflection coefficients, which are integral quantities, is far from a crucial test of the theory.

3. Data on Forward Scattering over the Sea

Here again our purpose is only to comment on a few examples of this type of data, rather than attempt any survey. The experiment summarized by Beard (1961) shows many good features in terms of comparing theory with experimental measurement. A number of properties of the

scattered radiation were measured, including a division into coherent and incoherent portions. The scattering surface was the ocean and various wave parameters were measured so as to characterize the surface by the "apparent ocean roughness" parameter ($h\gamma/\lambda$), where h = rms wave height, γ = grazing angle, and λ = wavelength. Thus the experimental data, gathered on transmissions between oil drilling platforms in the Gulf of Mexico, could readily be compared to the theoretical predictions available in 1961. It is worthwhile to point out that the experiments were planned by one laboratory but executed by another organization in close cooperation. Possible future experiments might well benefit from the combined talents of two organizations.

The measurement of both coherent and incoherent components of the scattered wave was an attempt to isolate the radiation scattered by a "diffuse" scattering mechanism. Clearly this was a good idea for application to low-angle radar tracking.

From the viewpoint of more modern ideas in scattering theory, these Gulf of Mexico experiments were inadequate in a number of respects. However, our comments here should not be taken as criticism of the original work; but rather as ideas as to how a future experiment along similar lines might be made more pertinent to current scattering theory. Concerning the scattered-wave measurements, a more nearly complete characterizatien of the scattered wave is needed. For example, Tyler and Howard (1973) measured the deterministically polarized and randomly polarized portions of electromagnetic waves forward-scattered from the lunar surface. This measurement was an attempt to separate radiation scattered by a "quasi-specular" process, which is relatively well understood, from that scattered by a "diffuse" process, which is not well understood (see Section II-B). Also, the characteristics of the ocean surface need to be more carefully

measured. For example, the rms wave height was measured in the Gulf of Mexico experiment, while the rms wave slope is the quantity needed to relate to quasispecular theory. The characterization of the surface roughness also needs to be specified over a range of horizontal distance scales both larger and smaller than the wavelength.

4. Lunar Bistatic Radar Experiment

Tyler and Howard (1973) investigated the lunar surface using S-band and VHF transmitters on the Apollo (14, 15, and 16) command modules and Earth-based receivers in a bistatic, CW radar experiment. The experiment geometry is shown in Figure 8. They have kindly provided some of the Apollo 16 S-band data for use in this report. One of the unique features of the experiment was the measurement of the coherency matrix of the scattered radiation. This was accomplished in practice by recording the complex components of both the right- and the left-circularly polarized portions of the scattered radiation. From this basic measurement the scattered signal could be resolved into a deterministically polarized (or "polarized") portion associated with the quasispecular scattering mechanism and a randomly polarized (or "unpolarized") portion associated with one or more "diffuse" scattering mechanisms. When adjusted to normal incidence, the ratio of "polarized" to "unpolarized" power was between 5 and 9 dB at S-band. Thus, quasispecular scattering is the dominant mechanism at this frequency. Interpreting the "polarized" component of scattered radiation as being due to the quasispecular scattering mechanism, the experimenters were able to determine the rms slope and dielectric constant of the near-specular region as it moved across the lunar surface with the motion of the command module.

Lunar slope measurements based on bistatic radar observations at 2.2 m wavelength have been compared with photographic results (Tyler

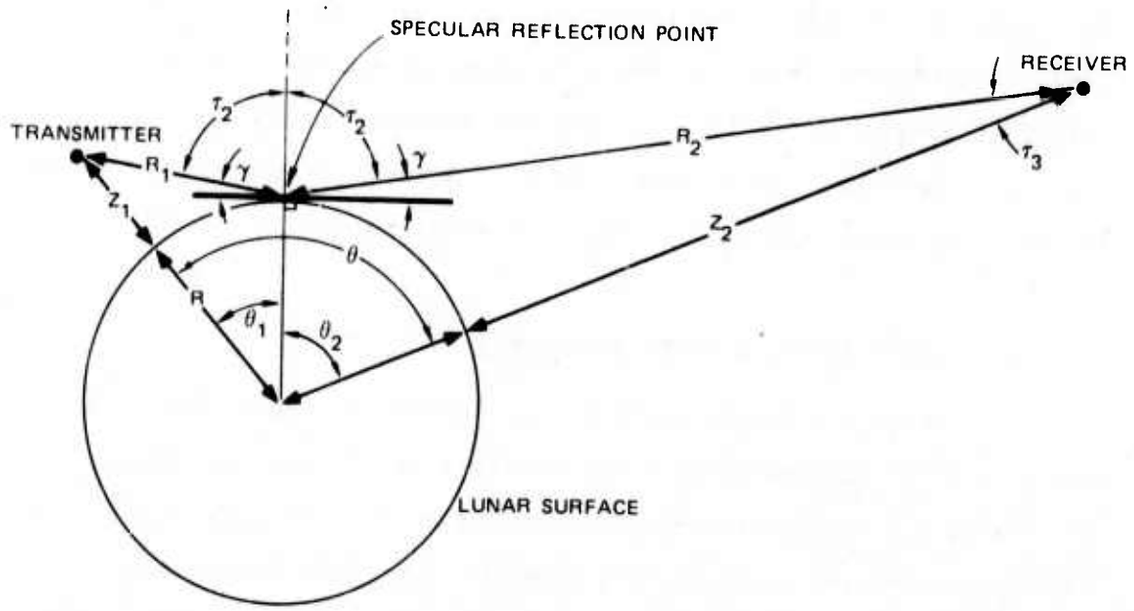

FIGURE 8 SCATTERING GEOMETRY FOR APOLLO 16 BISTATIC RADAR EXPERIMENT. For the moon, R = 1738 km.

et al., 1971). The photographic and bistatic radar methods are in agreement provided the bistatic radar scale length L can be adjusted over a range of about ± 20%. This successful "ground truth" verification of bistatic radar methods lends credibility to the analysis which follows.

Using the "polarized" component of the scattered signal and knowing the experimental conditions, Tyler and Howard (1973) inferred a power reflectivity (ρ^2) for the lunar surface by assuming a quasispecular scattering mechanism. This inferred reflectivity is the quantity used for comparison with theory later in this section (Figures 9 and 10). Though ρ^2 is known only to within a multiplicative constant, we will not find this a serious drawback because the data cover a wide range of grazing angles.

This bistatic lunar radar data is of particular interest here because it can be compared to the shadowing theory of Section II-B-4 with a relative minimum of uncertainty. In addition, the data cover a range

of grazing angles from 80° to 2.5°. Clearly, a detailed comparison of lunar data with scattering theory is beyond the scope of this report. Rather, our purpose here is to show the importance of shadowing effects at small grazing angles and to suggest approaches for more definitive work.

The theoretical value of the power reflection coefficient is taken to be of the form

$$\rho^2 = C\, D^2\, \tilde{Q}\, \tfrac{1}{2}(R_\perp^2 + R_\parallel^2) \tag{20}$$

where C is a normalizing constant, D^2 is the divergence factor, $\tilde{Q}$ is the shadowing function, and $\frac{1}{2}(R_\perp^2 + R_\parallel^2)$ is the classical Fresnel reflection coefficient for power. For the geometries of interest here, Tyler and Ingalls (1971) have shown that to first order a quasispecular scattering law gives results equivalent to the Fresnel coefficient used in Eq. (20) above. Hence we have used the simpler Fresnel expression. The methods by which each of the factors was calculated are described briefly below.

When a wave scatters from a convex spherical surface as opposed to a plane surface, the curvature of the surface causes the paths of reflected rays to diverge. Thus, an observer receives less scattered power from a convex surface than he would from an equivalent plane surface. This divergence effect is taken into account by the divergence factor D^2 in Eq. (20). The geometry is illustrated in Figure 8, where we have assumed specular scattering. Kerr et al. (1951, p. 406) quote a result of Van de Pol and Bremmer (1939) giving

$$D^2 = \frac{R^2 (R_1+R_2)^2 \sin \tau_2 \cos \tau_2}{[(R+Z_2)\, R_1 \cos \tau_3 + (R+Z_1)\, R_2 \cos \tau_1](R+Z_1)(R+Z_2)\sin \theta} \tag{21}$$

Given the experimental geometry, application of the law of sines yields all the parameters to find D^2 from Eq. (21).

The inferred reflectivity ρ^2 measured by Tyler and Howard (1973) has been adjusted to take the Moon's spherical shape into account and thus their values of ρ^2 given in Figures 9 and 10 refer to a scattering surface which is, on the average, flat. Hence, in calculating theoretical values of ρ^2 to compare with the bistatic radar measurements, we have used the divergence factor appropriate to a flat surface ($D^2 = 1$) in Eq. (20).

The shadowing function $\tilde{Q}$ takes account of the fact that one portion of a rough surface can shadow another, especially at low grazing angles. A knowledge of the grazing angle ($\gamma = \gamma_i = \gamma_s$) and the unidirectional rms slope ($\tan \beta_o$) determines $\tilde{Q}$ via Eqs. (6) and (11).

The classical Fresnel reflection coefficients for electric-field components perpendicular to and parallel to the plane of incidence are, respectively,

$$R_\perp = \frac{\sin\gamma - (\epsilon - \cos^2\gamma)^{\frac{1}{2}}}{\sin\gamma + (\epsilon - \cos^2\gamma)^{\frac{1}{2}}} \tag{22}$$

and

$$R_\parallel = \frac{\epsilon \sin\gamma - (\epsilon - \cos^2\gamma)^{\frac{1}{2}}}{\epsilon \sin\gamma + (\epsilon - \cos^2\gamma)^{\frac{1}{2}}} \tag{23}$$

where ϵ is the average dielectric constant. To obtain the classical reflection coefficient for power, we need to know the polarization of the incident wave. In the case examined here the incident wave is approximately equally divided between parallel and perpendicular components, so we use $\frac{1}{2}(R_\perp^2 + R_\parallel^2)$. The average dielectric constant ϵ is assumed to be 3 in all cases for the lunar surface. Values between 2.8 and 3.1 have been observed, however.

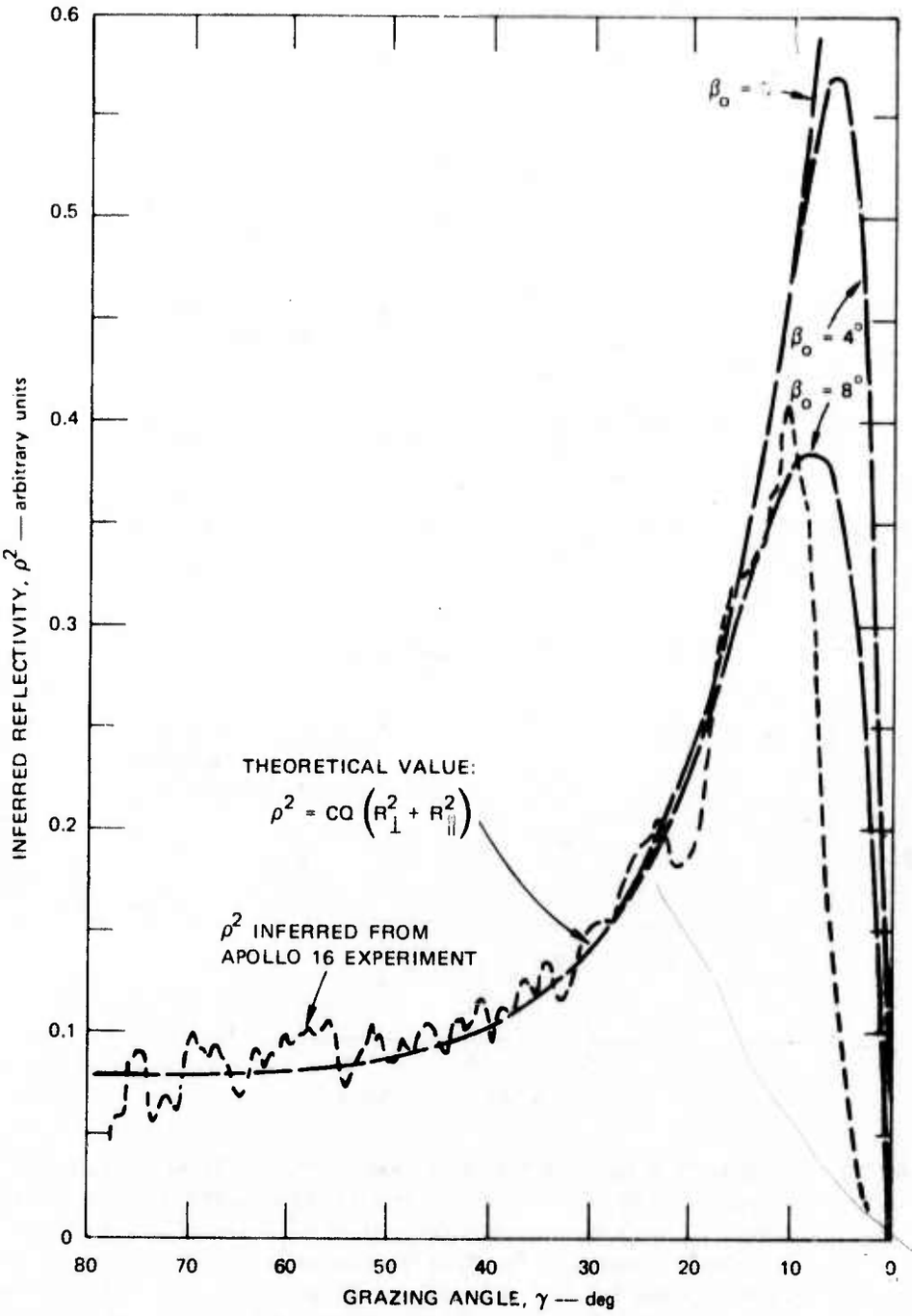

FIGURE 9 COMPARISON OF THEORETICAL AND EXPERIMENTAL VALUES FOR THE POWER REFLECTIVITY (ρ^2) OF THE LUNAR SURFACE. The ordinate scale is arbitrary since the experimental value of ρ^2 is known only to within a multiplicative constant. Tan β_o is the unidirectional rms slope of the lunar surface assumed for the theoretical calculations of ρ^2. The Apollo 16 data (———— line) were kindly provided by Dr. G. L. Tyler of the Stanford Center for Radar Astronomy.

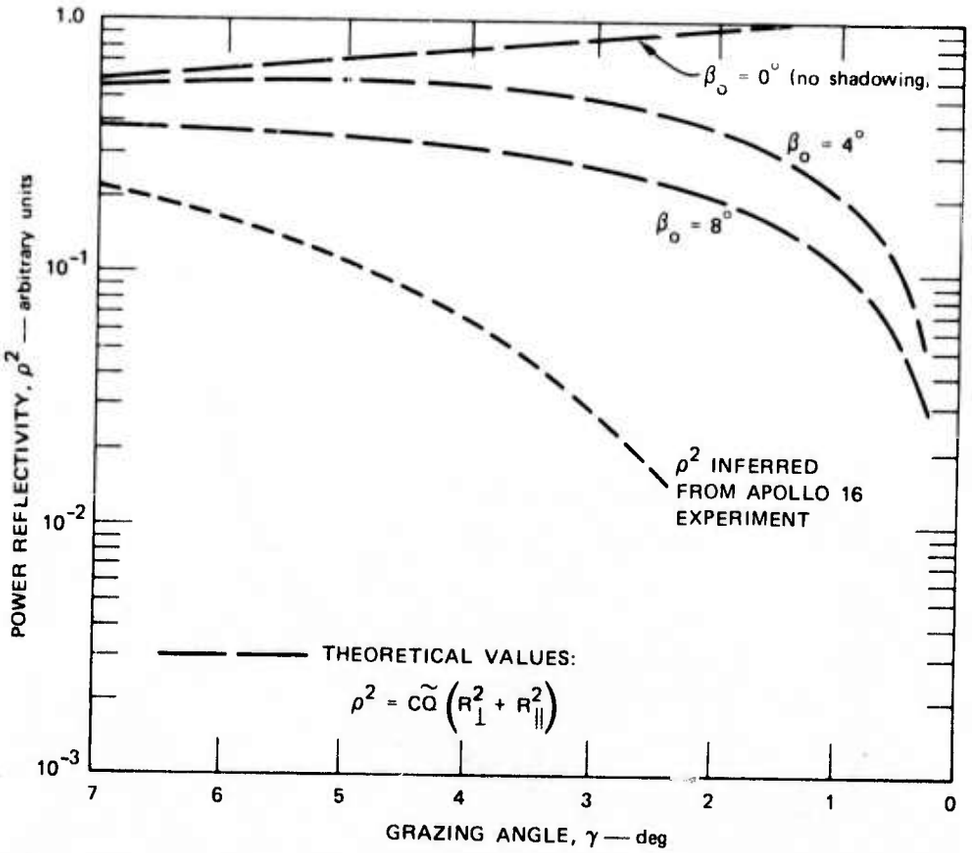

FIGURE 10 COMPARISON OF THEORETICAL AND EXPERIMENTAL VALUES FOR THE POWER REFLECTIVITY (ρ^2) OF THE LUNAR SURFACE. The ordinate scale is arbitrary, since the experimental value of ρ^2 is known only to within a multiplicative constant. Tan β_o is the unidirectional rms slope of the lunar surface assumed for the theoretical calculations of ρ^2. This semi-log presentation for grazing angles between 0° and 7° allows a closer examination of the role of shadowing at small grazing angles. The Apollo 16 S-band data (———— line) were kindly provided by Dr. G. L. Tyler of the Stanford Center for Radar Astronomy.

The theoretical values of ρ^2, based on Eq. (20), and the Apollo 16 bistatic radar measurements of ρ^2 are compared in Figures 9 and 10. Since the experimental values of ρ^2 are known only to within a mulitplicative constant we cannot compare the theoretical and experimental values on an absolute basis. However, by setting the normalizing constant C such that the theoretical curves match the experimental curve at near normal incidence ($\gamma = 80^\circ$), the shapes of the two curves can be compared. This particular normalization is chosen so as to make the experimental and theoretical curves agree at large grazing angles where shadowing effects are unimportant. No significance should be attached to the value of C since the vertical scale in Figures 9 and 10 is an arbitrary one. To use Eq. (20) elsewhere, as a model for the calculation of ρ^2 in an absolute sense, C should be taken as unity.

The three theoretical curves differ only in the value of rms unidirectional slope (tan β°) used to calculate the shadowing factor $\tilde{Q}$. The curve for $\beta_o = 0^\circ$ includes no shadowing effects--i.e., $\tilde{Q} = 1$ in Eq. (20). It allows one to judge the relative importance of the shadowing function $\tilde{Q}$. On the Moon values of β_o range from about 2° to 4° for the relatively smooth maria to about 4° to 8° for the relatively rough highland regions. Thus the curves for $\beta_o = 4^\circ$ and 8° plotted in Figures 9 and 10 correspond to rather rough mare and highland terrain respectively. For comparison the value of β_o for the Sierra Nevada mountains in California is roughly 7°.

The scattering region to which the measurements of ρ^2 apply moves across the lunar surface with the movement of the transmitter in the command module. Each point along the track of the scattering region corresponds to a different value of γ because the experimental geometry changes with transmitter movement. Thus measurements of ρ^2 at different values of γ in Figures 9 and 10 correspond to different scattering regions on the lunar surface. For high values of γ the scattering region is

located near the center of the lunar disk passing near the craters Descartes and Ptolemaeus as γ moves to lower values. As γ continues to decrease, the scattering region moves across the southern end of Oceanus Procellarum and finally over the western limb. For low grazing angles, which are of principal interest here, the scattering region is the lunar highlands near the western limb. Hence a value of β_o from 6° to 8° is appropriate to the interpretation of Figures 9 and 10 for $\gamma \leq 10^\circ$.

At large grazing angles ($\gamma \geq 15^\circ$) agreement between the experimental and theoretical curves of Figure 9 is excellent. Below $\gamma = 15^\circ$ the experimental curve for $\beta_o = 8^\circ$ agrees most closely with the experimental data and the theoretical curve without shadowing ($\beta_o = 0^\circ$) becomes obviously incorrect. The fact that the $\beta_o = 8^\circ$ curve is a better fit than the curve for $\beta_o = 4^\circ$ is expected since for $\gamma \leq 10^\circ$ the scattering region on the lunar surface is a relatively rough highland region where one expects to find β_o in the 6° to 8° range.

At small grazing angles ($\gamma < 10^\circ$) the experimental curve falls progressively further below the theoretical curves. In Figure 10 this feature is shown in more detail. The main difference between the theoretical curve for $\beta_o = 8^\circ$ and the experimental curve in Figure 9 is that the experimental curve breaks downward more sharply and at a larger value of γ than the theoretical one. The most probable explanation for this phenomenon appears to be the neglect of a particular type of multiple scattering in the theoretical model of Eq. (20). In the model of Eq. (20) waves that are scattered toward the receiver by a properly tilted facet are only shadowed to the extent that a random fluctuation from a mean plane surface may intercept them. That is, the shadowing model does not include the effect of surface curvature. Thus waves that scatter from properly tilted facets on the transmitter side of the specular point and that escape shadowing by random surface fluctuations are assumed to propagate to the receiver. In reality the ray path of such a wave may intersect

the curved lunar surface and be deflected by a second scattering. Further work on this "bulk shadowing" effect is needed to bring the theory of scattering at low grazing angles into better agreement with the experimental measurements given in Figures 9 and 10. It is worthwhile to point out that the radius of curvature of the Earth is nearly four times that of the Moon, so the "bulk shadowing" effect would be of reduced importance for the Earth's surface.

From this brief comparison of theory and experiment several conclusions can be drawn. First, the quasispecular scattering theory without shadowing is quite acceptable for $\gamma > 15^\circ$. However, for $\gamma < 15^\circ$ shadowing plays an increasingly important role and should be included in the scattering model. For $15^\circ \geq \gamma \geq 10^\circ$ the shadowing theory of Bass and Fuchs [Eqs. (6) and (11)] is adequate to explain the experimental data, but for $\gamma < 10^\circ$ the experimental value of ρ^2 falls more rapidly than the shadowing theory predicts. This failure of the scattering model is thought to be due to "bulk scattering" by the curved surface of the Moon. Further work to include "bulk scattering" in the model of Eq. (20) is needed to bring theory and experiment into better agreement for $\gamma < 10^\circ$. Work on the inclusion of "bulk shadowing" is now underway.

To sum up the shadowing theory of Bass and Fuchs makes a very necessary improvement in the scattering model at low grazing angles ($\gamma < 15^\circ$). However, it is thought that "bulk shadowing" must also be included for grazing angles below about 10°.

D. Relevance of Scattering Theory to Low-Angle Radar Tracking

There are roughly three routes by which improvements in scattering theory will manifest themselves as improvements in low-angle radar performance. First, an accurate scattering theory will allow accurate estimates of low-angle elevation errors for existing radars, since

multipath reflection effects are the major source of error at low angles. Next, a good scattering theory will enable us to evaluate new schemes for reducing errors--for example, by using state space modeling to optimize the radar system as a whole. Indeed, features revealed by a good scattering theory may well suggest new methods of reducing errors. Finally, a sufficiently good scattering theory might enable one to correct at least partially for multipath errors through sophisticated data processing.

1. Error Estimation

Hey and Parsons (1955) and Evans (1966) make elevation-error estimates using specular reflection models and compare their estimates with experimental error measurements. While the theory does suggest the main features of the measurements, it is clearly not accurate enough to make corrections. Barton (1974) does an analysis of low-angle elevation errors using a more sophisticated model that includes "diffuse" as well as specular scattering. He concludes that approaches exist that will allow 0.1 antenna beamwidth rms accuracy in elevation angle at elevation angles as low as $\frac{1}{4}$ beamwidth. The "diffuse" scattering theory used by Barton (1974) is a quasispecular theory modified by a "roughness factor." An experiment has been proposed by Armstrong et al. (1974) to test Barton's theory. Obviously, the more accurate the scattering theory is, the more accurate will be the error estimates for a given radar system.

2. Evaluation and Synthesis of New Techniques

The specular reflection theory used by Hey and Parsons (1955) and by Evans (1966) suggested to them techniques for error reduction that they then tried in practice. For example, Evans tried erecting 12-ft-by-12-ft shielding screens at the specular point to reduce multipath errors. The screens did, in fact, reduce the elevation errors by about a factor of two for an elevation angle of about 2°.

Evans (1966) notes that during experiments at X-band frequencies the mowing of 1-ft-long grass in the scattering region increased the measured reflection coefficient by a factor of about 4. Such interesting facts have suggested that modification of the scattering terrain in front of a radar might be worthwhile in terms of error reduction--especially something as easy as not mowing grass. This topic is discussed at more length in Section III. In any case, a critical theoretical analysis of radar siting and terrain modification as useful error-reduction techniques requires an accurate scattering theory.

A good scattering theory is also required for an overall study of a given radar system--for example, by the Kalman filtering approach discussed in Section III-B-2-i below.

3. Error Correction

A straightforward acceptance of the simple specular reflection model used by Hey and Parsons (1955) and Evans (1966) leads one to expect that a correction algorithm could be developed for multipath errors. Unfortunately, the situation is sufficiently complicated that Evans concluded such a scheme to be, in general, impractical. More recently, White (1974) has successfully developed a system that greatly reduces the effects of multipath over water. His system, which models the multipath effect by assuming specular reflection, is discussed in more detail in Section III-B-2. However, were a more accurate scattering theory available it would presumably be possible to use the theory to make better corrections, or simply to use the incoming data in a new and different way. Present and future electronic hardware will make possible swift, economical, and reliable computation. So even a rather complicated scattering theory could be exploited.

III RADAR SYSTEMS FOR LOW-ANGLE TRACKING

A. General

There are many system configurations and system techniques that may be applied so as to achieve good low-angle tracking by radar systems. Depending on the particular application and the desired performance level, various combinations of these techniques may be employed. In Section III-B-1 below, the general radar design parameters are examined relative to tracking low-altitude targets. Section III-B-2 examines various system techniques that may be applied to improve both new designs and existing installations.

In much of what follows, it is assumed that a sufficiently good model exists for the scattering of radar signals from the surrounding terrain. For the present we will use the quasispecular model with shadowing discussed in Section II above. However, as indicated in Section II, further work is needed in developing a low-angle scattering model. Such developments may be needed before some of the techniques in this section can be applied.

B. Radar System Design for Low-Altitude Tracking Ability

There are two basic approaches that can be applied to achieve low-altitude tracking ability. The first is basically a "brute force" approach in which the basic radar is designed with sufficient bandwidth, power, and antenna aperture to separately resolve the low-altitude target from any possible image created by the scattering of the return signal from the surrounding surface. The second approach is to accept the fact that multipath scattering of the target return signal is going to occur. A model of this scattering process is then developed and used in the processing of

the returned signals to adjust the radar, estimate the target parameters, and estimate the model parameters so that the multipath effect can be taken into account. This second approach may be applied after the first approach has been employed, or it may be applied in order to update some existing installations. In a recent, useful review paper, Barton (1974) discusses most of the possibilities of the first approach but does not cover many of the possibilities of the second approach. Thus the emphasis of this chapter will be primarily on the second approach. One should bear in mind, while considering these signal-processing schemes, that large-scale integrated-circuit (LSI) technology has made and will continue to make (for at least the next 5 to 10 years) data processing equipment smaller, lighter, cheaper, and more reliable. Thus rather sophisticated data-processing schemes that might have been prohibitive in the past due to size, expense, or reliability considerations may well be possible now.

1. Brute-Force Methods

a. Antenna Aperture

Perhaps the most obvious way to separate a target signal and its images caused by scattering from the terrain is to increase the antenna aperture until sufficient angular resolution is obtained to track the target and reject signals scattered by the terrain. The expression for the half-power beamwidth of an antenna array of aperture (length) ℓ is given by Jasik (1961, p. 2-24) as

$$\theta_{HP} = \frac{A\lambda}{\ell} \tag{24}$$

where λ is the wavelength, and A is the constant that varies slightly depending on the desired sidelobe level. For our purposes, A can be chosen as 1 where θ_{HP} is in radians. This corresponds to -25 dB sidelobe levels for a Dolph-Tchebyscheff array. If f is the radar frequency, then

$$\lambda = c/f \tag{25}$$

and

$$\theta_{HP} = c/f\ell \quad . \tag{26}$$

Now θ_{HP} is also approximately the angular distance from the antenna pattern maximum to the first null; so setting θ in Figure 11 equal to θ_{HP} we have

$$\ell \approx c/\theta f \tag{27}$$

as the minimum antenna aperture necessary to suppress the reflected signal while the target is in the center of the main lobe. It is theoretically possible to obtain a considerably narrower main lobe; however, all such "super gain" designs have failed in practice for what are now well understood reasons, as explained by Buck and Gustincic (1967). The angle θ is easily found from the flat Earth radar/target geometry of Figure 11 as

$$\theta = \tan^{-1}[(h_t - h_r)/G] + \tan^{-1}[h_r/X_s] \quad . \tag{28}$$

The present assumption about the scattering process is that the reflected angle γ_s is equal to the incident angle γ_i. Thus we may find $\tan^{-1}(h_r/X_s)$ as follows:

$$\frac{h_r}{X_s} = \frac{h_t}{T} = \frac{h_r + h_t}{X_s + T} \tag{29}$$

but

$$G = X_s + T \tag{30}$$

hence,

$$\frac{h_r}{X_s} = \frac{h_r + h_t}{G} \tag{31}$$

or

$$\theta = \tan^{-1}[(h_t - h_r)/G] + \tan^{-1}[(h_r + h_t)/G] \quad . \tag{32}$$

The antenna aperture ℓ necessary to reject the reflected return signal may now be determined. The results of this calculation are illustrated in the last column of Tables 1(a) through 1(f) and were produced with the computer program given in the appendix.

The difficulty of constructing large antennas grows roughly as ℓ^3 (since antennas are three-dimensional structures). Thus, large antennas become very expensive and impractical for very large apertures. For example, from Table 1 note that for a range of 54 km, an 8-m antenna aperture is required for a 10-GHz radar system elevated 10 m, tracking a target at an elevation of 100 m. Other configurations of target and antenna height are illustrated and may be used to determine the feasibility of improving low-altitude tracking by increasing the antenna aperture.

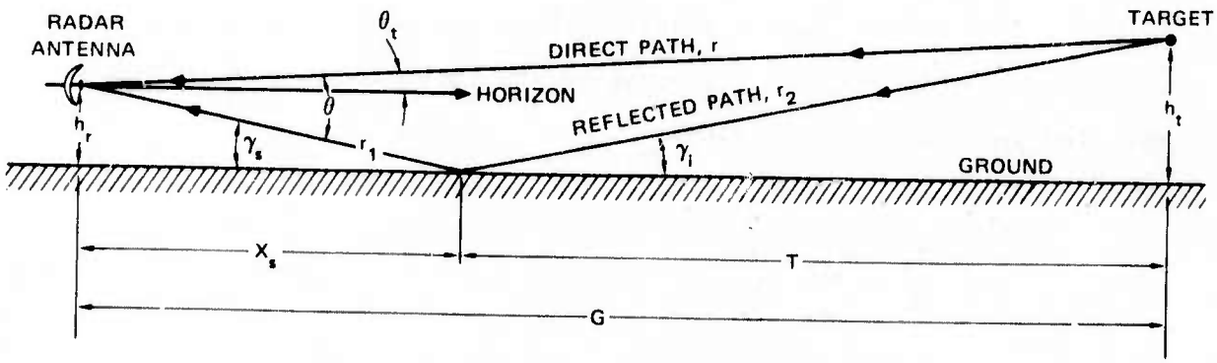

FIGURE 11 RADAR ANTENNA/TARGET GEOMETRY

Table 1

LOW-ALTITUDE RADAR SCATTERING PARAMETERS

(a) Radar frequency (f) = 10 GHz.
Unidirectional rms slope of scattering surface (tan β_o) = 0.0.
Radar antenna height (h_r) = 10 m.
Target height (h_t) = 100 m.

Target Range, r* (m)	Difierential Time Delay, δ (ns)	Range to Scattering Point, r_1 (m)	Angle, θ (rad)	Amplitude Ratio (Scattered/ Direct)	Required Antenna Aperture, ℓ (m)
2,000	3.3313	181	0.099914	0.741	0.300
4,000	1.6672	363	0.049989	0.858	0.599
6,000	1.1116	545	0.033330	0.902	0.899
8,000	0.8338	727	0.024999	0.925	1.199
10,000	0.6670	909	0.019999	0.940	1.499
12,000	0.5559	1090	0.016666	0.949	1.798
14,000	0.4764	1272	0.014285	0.956	2.098
16,000	0.4169	1454	0.012500	0.962	2.398
18,000	0.3706	1636	0.011111	0.966	2.698
20,000	0.3335	1818	0.010000	0.969	2.998
22,000	0.3032	2000	0.009091	0.972	3.297
24,000	0.2779	2181	0.008333	0.974	3.597
26,000	0.2565	2363	0.007692	0.976	3.897
28,000	0.2382	2545	0.007143	0.978	4.197
30,000	0.2223	2727	0.006667	0.979	4.497
32,000	0.2084	2909	0.006250	0.980	4.796
34,000	0.1962	3090	0.005882	0.981	5.096
36,000	0.1853	3272	0.005556	0.982	5.396
38,000	0.1755	3454	0.005263	0.983	5.696
40,000	0.1667	3636	0.005000	0.984	5.996
42,000	0.1588	3818	0.004762	0.985	6.295
44,000	0.1516	4000	0.004545	0.985	6.595
46,000	0.1450	4181	0.004348	0.986	6.895
48,000	0.1389	4363	0.004167	0.987	7.195
50,000	0.1334	4545	0.004000	0.987	7.495
52,000	0.1282	4727	0.003846	0.988	7.794
54,000*	0.1235	4909	0.003704	0.988	8.094

*The table has been terminated when the target would be below the horizon for a curved Earth with standard atmospheric refraction.

Table 1 (Continued)

LOW-ALTITUDE RADAR SCATTERING PARAMETERS

(b) Radar frequency (f) = 10 GHz,
Unidirectional rms slope of
scattering surface ($\tan \xi_0$) = 0.0,
Radar antenna height (h_r) = 10 m,
Target height (h_t) = 200 m.

Target Range, r (m)	Differential Time Delay, (ns)	Range to Scattering Point, r_1 (m)	Angle, ζ (rad)	Amplitude Ratio (Scattered/Direct)	Required Antenna Aperture, ℓ (m)
2,000	6.6379	95	0.199332	0.575	0.150
4,000	3.3323	190	0.099916	0.751	0.300
6,000	2.2224	285	0.066642	0.824	0.449
8,000	1.6672	380	0.049990	0.864	0.599
10,000	1.3339	476	0.039995	0.889	0.749
12,000	1.1116	571	0.033330	0.906	0.899
14,000	0.9529	666	0.028569	0.919	1.049
16,000	0.8338	761	0.024999	0.929	1.199
18,000	0.7411	857	0.022221	0.936	1.349
20,000	0.6670	952	0.019999	0.942	1.499
22,000	0.6064	1047	0.018181	0.947	1.648
24,000	0.5559	1142	0.016666	0.951	1.798
26,000	0.5131	1238	0.015384	0.955	1.948
28,000	0.4764	1333	0.014285	0.958	2.098
30,000	0.4447	1428	0.013333	0.961	2.248
32,000	0.4169	1523	0.012500	0.963	2.398
34,000	0.3924	1619	0.011765	0.965	2.548
36,000	0.3706	1714	0.011111	0.967	2.698
38,000	0.3511	1809	0.010526	0.968	2.848
40,000	0.3335	1904	0.010000	0.970	2.998
42,000	0.3176	2000	0.009524	0.972	3.147
44,000	0.3032	2095	0.009091	0.973	3.297
46,000	0.2900	2190	0.008696	0.974	3.447
48,000	0.2779	2285	0.008333	0.975	3.597
50,000	0.2668	2380	0.008000	0.976	3.747
52,000	0.2565	2476	0.007692	0.977	3.897
54,000	0.2470	2571	0.007407	0.978	4.047
56,000	0.2382	2666	0.007143	0.979	4.197
58,000	0.2300	2761	0.006897	0.979	4.347
60,000	0.2223	2857	0.006667	0.980	4.497
62,000	0.2151	2952	0.006452	0.981	4.646
64,000	0.2084	3047	0.006250	0.981	4.796
66,000	0.2021	3142	0.006061	0.982	4.946
68,000	0.1962	3238	0.005882	0.982	5.096
70,000*	0.1906	3333	0.005714	0.983	5.246

*The table has been terminated when the target would be below the horizon for a curved Earth with standard atmospheric refraction.

Table 1 (Continued)

LOW-ALTITUDE RADAR SCATTERING PARAMETERS

(c) Radar frequency (f) = 10 Ghz.
Unidirectional rms slope of scattering surface ($\tan \beta_o$) = 0.0.
Radar antenna height (h_r) = 10 m.
Target height (h_t) = 300 m

Target Range, r (m)	Differential Time Delay, τ (ns)	Range to Scattering Point, r_1 (m)	Angle, θ (rad)	Amplitude Ratio (Scattered/Direct)	Required Antenna Aperture, ℓ (m)
2,000	9.8958	64	0.297773	0.455	0.100
4,000	4.9893	129	0.149719	0.660	0.200
6,000	3.3310	193	0.099917	0.754	0.300
8,000	2.4999	258	0.074965	0.807	0.399
10,000	2.0004	322	0.059982	0.842	0.499
12,000	1.6672	387	0.049990	0.866	0.599
14,000	1.4291	451	0.042851	0.883	0.699
16,000	1.2506	516	0.037496	0.897	0.799
18,000	1.1116	580	0.033330	0.908	0.899
20,000	1.0005	645	0.029998	0.916	0.999
22,000	0.9096	709	0.027271	0.924	1.099
24,000	0.8338	774	0.024999	0.930	1.199
26,000	0.7696	838	0.023076	0.935	1.299
28,000	0.7147	903	0.021428	0.939	1.399
30,000	0.6670	967	0.019999	0.943	1.499
32,000	0.6253	1032	0.018749	0.947	1.599
34,000	0.5886	1096	0.017647	0.950	1.698
36,000	0.5559	1161	0.016666	0.952	1.798
38,000	0.5266	1225	0.015789	0.955	1.898
40,000	0.5003	1290	0.015000	0.957	1.998
42,000	0.4764	1354	0.014285	0.959	2.098
44,000	0.4548	1419	0.013636	0.961	2.198
46,000	0.4350	1483	0.013043	0.962	2.298
48,000	0.4169	1548	0.012500	0.964	2.398
50,000	0.4002	1612	0.012000	0.965	2.498
52,000	0.3848	1677	0.011538	0.966	2.598
54,000	0.3706	1741	0.011111	0.968	2.698
56,000	0.3573	1806	0.010714	0.969	2.798
58,000	0.3450	1870	0.010345	0.970	2.898
60,000	0.3335	1935	0.010000	0.971	2.998
62,000	0.3227	2000	0.009677	0.972	3.098
64,000	0.3127	2064	0.009375	0.973	3.197
66,000	0.3032	2129	0.009091	0.973	3.297
68,000	0.2943	2193	0.008823	0.974	3.397
70,000	0.2859	2258	0.008571	0.975	3.497
72,000	0.2779	2322	0.008333	0.976	3.597
74,000	0.2704	2387	0.008108	0.976	3.697
76,000	0.2633	2451	0.007895	0.977	3.797
78,000	0.2565	2516	0.007692	0.977	3.897
80,000	0.2501	2580	0.007500	0.978	3.997
82,000	012440	2645	0.007317	0.978	4.097
84,000*	0.2382	2709	0.007143	0.979	4.197

*The table has been terminated when the target would be below the horizon for a curved Earth with standard atmospheric refraction.

Table 1 (Continued)

LOW-ALTITUDE RADAR SCATTERING PARAMETERS

(d) Radar frequency (f) = 10 GHz.
Unidirectional rms slope of scattering surface (tan β_o) = 0.05.
Radar antenna height (h_r) = 20 m.
Target height (h_t) = 100 m.

Target Range, r (m)	Differential Time Delay, δ (ns)	Range to Scattering Point, r_1 (m)	Angle, θ (rad)	Amplitude Ratio (Scattered/ Direct)	Required Antenna Aperture, ℓ (m)
20,000	0.6671	3,333	0.010000	0.102	2.998
40,000	0.3335	6,666	0.005000	0.052	5.996
60,000*	0.2223	10,000	0.003333	0.035	8.994

(e) Radar frequency (f) = 10 GHz.
Unidirectional rms slope of scattering surface (tan β_o) = 0.05.
Radar antenna height (h_r) = 60 m.
Target height (h_t) = 300 m.

Target Range, r (m)	Differential Time Delay, δ (ns)	Range to Scattering Point, r_1 (m)	Angle, θ (rad)	Amplitude Ratio (Scattered/ Direct)	Required Antenna Aperture, ℓ (m)
20,000	2.0011	1,250	0.029998	0.252	0.999
40,000	1.0006	2,500	0.015000	0.134	1.998
60,000	0.6671	3,750	0.010000	0.091	2.998
80,000*	0.5003	5,000	0.007500	0.069	3.997

*The table has been terminated when the target would be below the horizon for a curved Earth with standard atmospheric refraction.

Table 1 (Concluded)

LOW-ALTITUDE RADAR SCATTERING PARAMETERS

(f) Radar frequency (f) = 10 GHz.
Unidirectional rms slope of scattering surface ($\tan \beta_o$) = 0.05.
Radar antenna height (h_r) = 60 m.
Target height (h_t) = 300 m.

Target Range, r (m)	Differential ime Delay, δ (ns)	Range to Scattering Point, r_1 (m)	Angle, θ (rad)	Amplitude Ratio (Scattered/ Direct)	Required Antenna Aperture, ℓ (m)
20,000	6.0033	3,333	0.029997	0.279	0.999
40,000	3.0019	6,666	0.015000	0.150	1.998
60,000	2.0013	10,000	0.010000	0.102	2.998
80,000	1.5009	13,333	0.007500	0.077	3.997
100,000	1.2007	16,666	0.006000	0.062	4.996

*The table has been terminated when the target would be below the horizon for a curved Earth with standard atmospheric refraction.

One way of increasing the effective antenna aperture without actually constructing a large dish antenna is to mount a series of small antennas on a receiving tower. This method is similar to the aperture-synthesis technique familiar in radio astronomy--cf. Christiansen and Högbom (1969), or Kraus (1969). Such a receiving tower would be effective only if the echo signal were sufficiently strong and improved resolution were required only in elevation (to discriminate against the image echo signal of Figure 1). In its simplest realization, such a tower would be about 100 m high, and would have several (one to ten) receivers

with wide-angle antennas strung out vertically along the tower. The tower, which may or may not be located near the transmitter, would not be difficult to construct and put in place; the main engineering requirement would be that the position of each of the receivers would have to be known to a fraction of the wavelength. (If the tower swayed, a correction could be made electronically if the magnitude of the swaying were measured in real time.) Such a receiver could give a resolution in the vertical direction of about $\lambda/d = 10^{-3}$ rad for a 100-m tower at 10 cm. There would, of course, be no useful resolution in the horizontal direction. For improved gain (at the price of a considerable increase in complexity) the antennas could have narrower beams and be made to sweep in the horizontal direction in synchronization with the transmitter. Or, the tower could be made higher with more receiving antennas.

It is also possible to fly the supplementary receiver from a balloon, rocket, airplane, or other airborne support, again only if its position is constantly monitored. Such monitoring could probably be achieved with three narrowband microwave transponders, chosen so as not to interfere with the radar return, and a simple computer. If a rocket were used, it would be launched only upon receipt of an interesting signal, with a receiver that would slowly drift down on a parachute or balloon. The data could be telemetered, or returned on a wire. The main disadvantage of a single receiver (or of a small number of receivers) is that the high resolution in the vertical direction would suffer from high sidelobes, which might require sophisticated processing. In a tower, with many receivers, these sidelobes could be made negligibly small through appropriate apodization.

b. Radar Operation at mm Wavelengths

In Eq. (24) we note that the half-power beamwidth (θ) of an antenna is given by $\theta \approx \lambda/\ell$. The previous section noted the improvements in low-angle radar performance that could be made by reducing θ through an increase in the antenna aperture (length) ℓ. Similar improvements could also be made by reducing the radar operating wavelength λ, thus avoiding the difficulties of large antenna structures. However, at frequencies above 40 GHz atmospheric attenuation begins to play an important role, and transmitting and receiving systems become less efficient. This and other applications of mm wavelength devices have been investigated by R. O. Hundley (1975).

Evans and Hagfors (1968, p. 391) give a convenient expression for the expected signal-to-noise ratio of a radar system. We can easily modify this expression to suit our purposes by introducing the factor $\exp(-2\alpha r)$ to account for atmospheric absorption. Letting the antenna gain, $G = 4\pi A_e/\lambda^2$, we have

$$\frac{P_r}{P_N} = \frac{P_t A_e^2 \sigma\, e^{-2\alpha r}}{4\pi r^4 \lambda^2 k T_s B}$$

where

P_r = received echo power

P_N = receiver system noise power

P_t = peak transmitted power

A_e = effective antenna area = $\pi(\ell/2)^2$

σ = target cross section

α = atmospheric attenuation coefficient

r = range to target

λ = radar system wavelength

T_s = receiver system noise temperature

B = receiver system bandwidth

and all are in SI (MKS units). Suppose we now require that our system have a 10 dB signal-to-noise ratio for low angle tracking, i.e., $(P_r/P_N) = 10$. Knowing the other parameters we can solve for the required transmitter peak power, P_t.

Taking nominal system parameters as follows:

$A_e = \pi(\ell/2)^2 = \pi/4$, i.e., antenna diameter, $\ell = 1$ m.

$\sigma = 0.1\ m^2$

$B = 0.1$ GHz

and using the above equation we can construct Table 2 below. The factors governing the parameter choices are discussed in due course.

Table 2

LOW-ANGLE RADAR TRACKING AT mm WAVELENGTHS

Target Range, r (m)	Radar Wavelength, λ (mm)	Atmospheric Attenuation Coefficient, α (m^{-1})	System Noise Temperature, T_s (K)	Antenna Beamwidth, θ (rad)	Required Transmitter Power, P_t (W)
20,000	10mm (=30GHz)	1.6×10^{-5}	650	0.01	4.4×10^{4}
50,000	10mm (=30GHz)	1.6×10^{-5}	650	0.01	4.4×10^{6}
20,000	1.35mm (=220GHz)	2.1×10^{-4}	2,700	0.00135	7.7×10^{6}
50,000	1.35mm (=220GHz)	2.1×10^{-4}	2,700	0.00135	9.0×10^{13}

Using Table 1 we can compare the low-angle tracking performance of the K_a band (30 GHz) and mm band (220 GHz) radars considered in Table 2. Looking in Table 1(a), for example, we find that for a radar situated 10 m above a flat Earth and tracking a target flying at 100 m altitude the K_a band radar of Table 2 will track out to a range of about 20 km. The mm wave radar by contrast will track virtually out to the horizon some 50 km away. This difference in performance is, of course, due to the extremely narrow beam pattern of our 1-m diameter dish at mm wavelengths. The superior performance of the mm wave radar is not achieved without effort however. The peak power required (P_t) is $\sim$ 200 times greater for the mm wave radar at r = 20 km and increases dramatically as r increases. The larger values of P_t required at the mm wavelength are due to increased receiver noise (higher T_s) and more importantly to the much greater amounts of atmospheric absorption (higher α). Atmospheric absorption varies strongly with frequency and the 1.35-mm wavelength is near a relative minimum. The r = 20 km values of P_t required in Table 2 are commensurate with current K_a band technology; but peak powers reliably available at around 1-mm wavelength fall in the 1 to 10 watt region, far below the requirements. We can therefore conclude that a significant improvement in low-angle radar performance can be obtained by going to a 10-mm wavelength (K_a band) within current technological limits. However, further significant improvements obtainable by going to $\sim$ 1-mm wavelengths will require a very large improvement in transmitter peak power! One can use pulse compression techniques to reduce the required peak power by a factor of up to 10^4. Even using pulse compression, substantial improvements in transmitter peak power must be realized to exploit the superior low-angle performance of a $\sim$ 1-mm wavelength radar.

The numbers quoted in Table 2 and the conclusions above are dependent on the parameter choices made, and, in particular, the values of α and T_s. Atmospheric absorption is due mainly to water vapor and oxygen molecules. The values of α used are for 1% water vapor and an atmospheric pressure of 760 mm of Hg. Absorption peaks due to molecular resonance bands make α a strong function of frequency. The particular operating wavelengths in Table 2 correspond to relative minima in atmospheric absorption. Skolnik (1962, p. 516) gives the plot of α versus wavelength from which the values of Table 2 were taken.

The system noise temperatures used in Table 2 are based on the use of microwave integrated circuits (MICs). While current MICs at 30 GHz (10 mm) can achieve a 5-dB noise figure (F), no MICs at 220 GHz (1.35 mm) have yet been constructed to the authors' knowledge. At the higher frequency, workers in the field think a 10-dB noise figure is achievable and lower values could probably be achieved with sufficient effort. The system noise temperature T_s was calculated using $T_s = T_o(F-1)$ where $T_o = 300^\circ K$. As can be seen from the equation above, the peak power required (P_t) is directly proportional to T_s; so the realization of a 1.35-mm radar could well be aided by lowering the system noise temperature through low-noise receiver development.

Another factor that will significantly influence mm wave radar performance is the accuracy to which the radar antenna can be constructed. At short wavelengths antenna surface tolerances become very close. Ruze (1952) considered the effects of parabolic dish distortion on antenna gain. For a worst case, the gain reduction is given by

$$\frac{G}{G_o} = 1 - \sigma^2$$

where

$$\sigma = \frac{4\pi d}{\lambda}$$

and d = rms surface deviation from true parabolic shape. Since the antenna gain (G) is related to the antenna beamwidth (θ) by $G = 4\pi\theta^2$, any significant reduction in antenna gain will significantly reduce low-angle tracking performance. For example, suppose we can construct an antenna surface to a tolerance (d) of 0.1 mm ($\sim 4 \times 10^{-3}$ in.). At λ = 10 mm (30 GHz), the gain reduction is about 0.1 dB and quite acceptable. If we try to use the same antenna at λ = 1.35 mm (220 GHz), the gain reduction is about 9 dB and θ increases by about 3 times, which could well be important.

In summary, mm wavelength radars can achieve good low-angle tracking performance by allowing one to obtain very narrow antenna beamwidths with relatively small antennas, such as the 1-m diameter dish considered in Table 2. However, as one operates at progressively higher frequencies, two factors require that the peak transmitter power P_t be progressively larger. These factors are the higher atmospheric attenuation and higher receiver noise temperature at higher frequencies. While the required effective peak power at 10 mm is within the current technology, P_t rises well above a megawatt at 1.35 mm for a target at 20-km range. Such a power level requires substantial increases in transmitter peak power capability at wavelengths around 1 mm in order to exploit the very much improved low-angle tracking performance achievable at these wavelengths. Improvements in receiver system noise temperature over the estimates used in Table 2 would also be helpful in reducing the required value of P_t, perhaps by as much as a factor of 4. It should also be noted that at short wavelengths--e.g., 1.35 mm--antenna surface tolerances become very tight indeed ($\sim$ 0.05 mm) if satisfactory performance is to be achieved.

c. Range Resolution

If the target must be tracked while the antenna pattern includes both the target and the horizon (due to insufficient antenna aperture), then the ability to determine the target altitude may be a function of the range resolution of the system. This occurs since range gates may be used in the tracking circuits to exclude the reflected signal if it can be separated in time from the direct target signal.

Thus, sufficiently short pulses will produce separate direct and scattered returns. Short pulses are associated with large bandwidths and it is easily shown [by Barton (1974), for example] that low-altitude tracking ability is proportional to the effective radar system bandwidth, whether it is implemented directly as suggested above or by pulse compression, frequency agility, FM sweeps, etc. Large system bandwidths are usually expensive, and for many systems of interest it is often insufficient to provide the desired low-altitude tracking capability.

The difference in arrival times of the direct and the reflected return is determined by the antenna, ground, and target geometry. The difference in path length for a flat Earth can be determined from Figure 11, as shown in Eqs. (33) and (34).

The direct path length is

$$r = \sqrt{G^2 + (h_t - h_r)^2} \tag{33}$$

while the reflected path length is

$$r_1 + r_2 = \sqrt{X_s^2 + h_r^2} + \sqrt{T^2 + h_t^2} \tag{34}$$

However, $G = X_s + T$ and $h_r/X_s = h_t/T$. Thus, the path difference, δ, is given by

$$\delta = r_1 + r_2 - r = \sqrt{h_r^2 + \left[G^2 h_r^2/(h_t + h_r)^2\right]}$$

$$+ \sqrt{h_t^2 + \left[G^2 h_t^2/(h_r + h_t)^2\right]} - \sqrt{G^2 + (h_t - h_r)^2} \qquad (35)$$

or

$$\delta = \sqrt{G^2 + (h_r + h_t)^2} - \sqrt{G^2 + (h_t - h_r)^2} \qquad (36)$$

and the time difference is δ/c where c is the velocity of light. The above function has been calculated and is given in the second column of Tables 1(a) through 1(f) for various parameters of the problem. The most apparent feature of the delay time is that for any target at long range, the difference in arrival times is very small, on the order of 0.1 ns. Thus, even extremely-wide-bandwidth radars could not directly separate the two signals in time.

d. Siting

The last brute-force method concerns the selection of a proper site for the radar. From Tables 1(a) through 1(f) it is apparent that a sufficiently large antenna height will provide any desired low-angle tracking capability. Very tall antennas are not always practical, so this technique is useful, but limited. The second site consideration is the surrounding terrain. Clearly, a perfectly smooth terrain would be a very good reflector of radar signals, while suitably rough surfaces could virtually eliminate the specularly scattered signal. Tables 1(d), (e), and (f) also illustrate the effect of surface roughness on the reflected

signal amplitude in the fifth column. The scattering model used is that of Eq. (20) with C = D = 1 and ϵ = 3 in Eqs. (22) and (23). Note that a unidirectional rms surface slope tan β_o of only 0.05 greatly attenuates the reflected return signal [see column 5 of Table 1(a) through 1(f)]. This calculation uses a very simple model, however, and as extensively discussed in Section II, all known low-angle scattering models are suspect.

2. Compensation Techniques for Low-Altitude Tracking

Once the basic radar parameters of frequency, bandwidth, antenna, aperture, and site have been fixed, then additional techniques may be applied to compensate for the reflected return signal.

a. Signal Processing and Measurements

The purpose of this subsection is to demonstrate that the difficulties of tracking a low-altitude target are mostly an artifact of the particular data-processing algorithm a monopulse radar uses, and that, with an appropriate but modest change in the monopulse radar configuration and processing algorithm, a radar can successfully track targets at low elevation angles.

Any processing algorithm presumes a definite model of the reflection coefficient from the ground (e.g., specular reflection and geometrical optics), and it is important to assess how sensitive such an algorithm is to deviations from the assumed reflection model. Such deviations will surely occur in real systems. For example, even smooth mirror surfaces (the ideal specular reflection) have corrections due to physical optics--i.e., Fresnel zones, when the radar is situated within a few antenna diameters of the surface.

The key question in the discussion to follow is, how many unknowns there are in the reflected radar signal, and how many measurements the radar must make to determine the unknowns. Clearly, in a multipath low-elevation-angle situation, the number of unknowns increases due to the reflected wave. The radar will then have to make more measurements to obtain information about the reflecting surface to identify the true elevation of the target.

In general, the idea is to express the properties of the reflecting surface according to a model that is specified by a small number of adjustable parameters (usually two or three). The number of receive beams on the radar is increased to permit two or three additional measurements, which then allows one to determine the adjustable perameters in the reflection coefficient and hence determine the bearing of the target.

First, let us see how these considerations work in a standard monopulse tracking scheme (Figure 12). Two signals, S_1 and S_2, are received whose amplitude and phase are given by

$$S_1 = A\, G(\theta_T - \theta_B - \Delta\theta)\, e^{2ikr} \tag{37}$$

$$S_2 = A\, G(\theta_T - \theta_B + \Delta\theta)\, e^{2ikr} \tag{38}$$

where r denotes the range; A is a complex amplitude determined by the range, the phase shift on reflection, the radar cross section of the target, and other factors; and G is the gain pattern of the radar antenna. Thus, there are four unknowns, r, Re(A), Im(A), and θ_T, and four measurements, the real and imaginary parts of S_1 and S_2, which allow us to determine the four unknowns. In particular, one employs the algorithm

$$\theta_T - \theta_B \propto \frac{S_1 - S_2}{S_1 + S_2} \tag{39}$$

to find the error signal that locates the target.

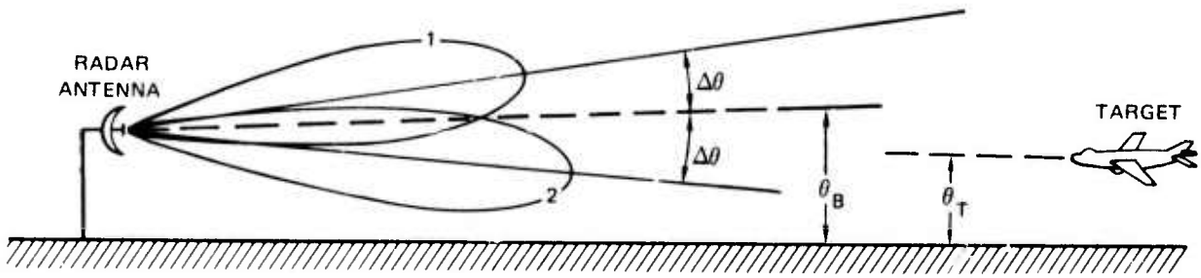

FIGURE 12 RECEIVE BEAMS OF A MONOPULSE RADAR. The upper beam is denoted by 1, while 2 denotes the lower beam. θ_B gives the boresight elevation angle of the radar, and the upper and lower beams are separated from the boresight direction by an angle $\Delta\theta$.

Now consider a three-beam system and reflection from the ground as shown in Figure 13. The i^{th} signal will then be

$$S_i = A_1 G(\theta_T - \theta_i)\, e^{2ikr} + \int_{-\frac{\pi}{2}}^{0} A(\theta)\rho(\theta)\, e^{i\psi(\theta)} G(\theta - \theta_i)\, d\theta \tag{40}$$

where A_1 represents the radiation from the target directly into the antenna and $A(\theta)$ the radiation that is received after ground reflection. The reflection coefficient is $\rho(\theta)\, e^{i\psi(\theta)}$.

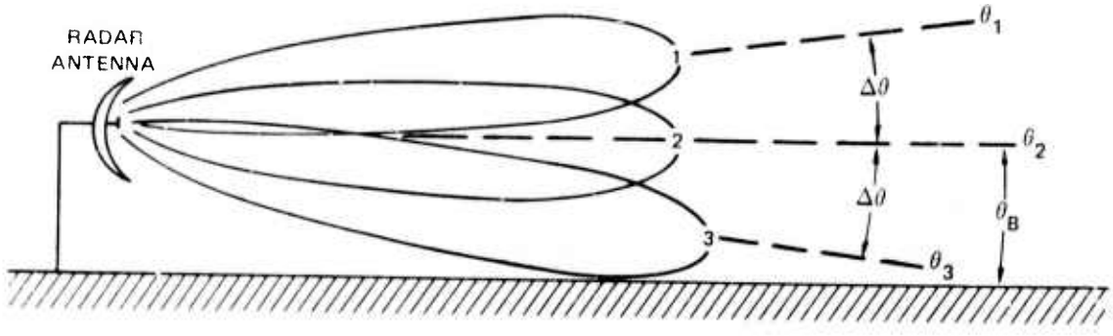

FIGURE 13 A THREE-BEAM RADAR. Such a system can distinguish between a target and its reflected image. θ_B is the boresight angle, and θ_i (i = 1, 2, 3) denote the pointing directions of the radar beams.

It is evident that if nothing is assumed to be known about the reflection coefficient, then each new measurement S_i (really two measurements--amplitude and phase), corresponding to a new value of θ_i, will only give two new pieces of information about the function $A(\theta)\rho(\theta)\, e^{i\psi(\theta)}$, which, in principle, has an infinite number of degrees of freedom. In such circumstances, we can never measure enough about the reflection coefficient to determine the target bearing.

Consequently, a reflection coefficient model must be adopted. The one mainly used so far is the specular-reflection/geometrical-optics approach whereby

$$\rho(\theta)\, e^{i\psi(\theta)} = \rho\, e^{i\psi}\, \delta(\theta + \theta_T - 2\theta_p) \tag{41}$$

where ρ is the reflection coefficient, ψ is the phase shift of the reflected ray relative to the direct ray, $\delta(\ )$ is the Dirac delta function, and θ_p is the inclination of the reflecting plane to the horizontal. This equation represents the reflection coefficient by a three-parameter model. In over-water applications, the parameters may be reduced to two by the assumption $\theta_T = 0$.

Each signal S_i is then given by

$$S_i = e^{ikr}\left[A_1 G(\theta_T - \theta_i) + A_2\rho e^{i\psi} G(2\theta_p - \theta_T + \theta_i)\right] \quad . \qquad (42)$$

We can suppose A_1 and A_2 to be real by absorbing any phase shifts into r and ψ. In this case, we have six unknowns, r, A_1, $A_2\rho$, ψ, θ_T and θ_p, and six measurements of amplitude and phas of S_i, i = 1, 2, 3. In principle, θ_T can be determined.

White (1974; see also Section IV) has used a restricted version of this scheme over water ($\theta_p = 0$ is assumed) wherein only the real parts of the signal are used.

The three unknowns are then A_1 cos kr, $A_2\rho$ and (kr + ψ), and θ_T, and the three measurements are $Re(S_i)$ = 1, 2, 3. Again, θ_T can be found. White's scheme shows that

$$\text{Error signal} \propto \theta_T^2 \qquad (43)$$

when θ_T is much less than a beamwidth, so that the signal-to-noise ratio is low when the elevation angle is low. But it is very important to point out that this processing algorithm keeps the errors bounded and the beam on the target.

It should be quite straightforward to modify existing monopulse radars to have low-altitude tracking capability. Figure 14 shows how feeds can be rearranged to achieve three vertical beams.

We have always supposed the reflection coefficient to be large ($\rho \sim 1$). In a particular air defense situation, the radars may be located in forest or other areas where the scattering is weak and diffuse leading to very little multipath. Our proposed schemes will work regardless of the value of ρ.

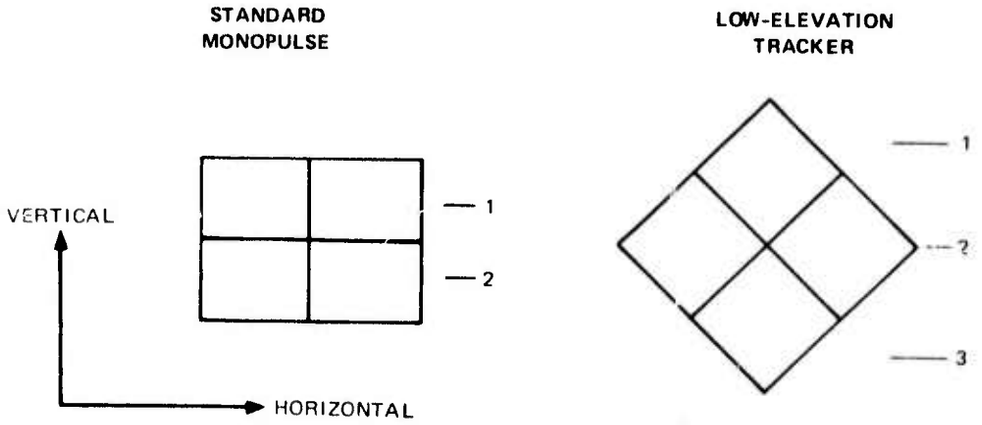

FIGURE 14 HORN ARRANGEMENT ON STANDARD MONOPULSE, AND LOW-ELEVATION TRACKER. The numbers refer to the antenna beams for the standard monopulse (Fig. 12) and three-beam (Fig. 13) radars.

In summary, modest modifications of existing radars will give them low-altitude tracking capability. But more work is required to find the optimum algorithms and to determine their sensitivity to various reflection-coefficient models. The further additional advantages of radar netting are examined below.

b. Radar Nets and Bistatic Operation

The netting together of several radar installations is a useful technique for improving overall system performance, including low-altitude tracking capability. Netting is useful in several respects and at several levels of complexity. First of all, one or more radar sites tracking the same target can mix (average) their vertical-scan error signals so as to effectively cancel tracking-error signals due to reflections that come from uncorrelated patches of terrain, while the direct signals from the target can be added coherently. This is a relatively simple procedure that can improve low-angle tracking, especially if more than two sites are tracking the same target, and is useful even if only one of the sites is transmitting. Multiple transmissions greatly improve the

tracking capability, however. For example, consider three monopulse radar sites (on separate frequencies) that are tracking the same target, but exchange information about return-pulse signal strength in the elevation sum and difference signals derived from each receiving antenna, and for each frequency. Let the parameters be defined as follows:

- Ψ_{mn} = Target reflection coefficient for the radar beam that is reflected from transmitter site m to receiver site n
- Φ_{mn} = Target reflection coefficient for the radar beam from transmitter m reflected in the direction of the reflecting surface for receiver site n
- ρ_n = Effective surface reflection coefficient between the target and receiver site n
- δ_n = Range difference between the direct and reflected signals from the target to receiver
- ω_m = Site m transmitter frequency (rad s^{-1})
- r_{mn} = Range from the target for the signal from transmitter m, as received by site n

Assume that sufficient knowledge and coordination is interchanged between radar sites. Then the target altitude can be estimated by forming a composite vertical-tracking error signal to drive all the antenna mounts together--i.e., form an equivalent error signal by simple averaging of the various combinations of returns.

To consider the enhancement in low-angle tracking capability due to this very simple (and no doubt non-optimal) averaging of the various radar signals, assume that the antennas are all tracking the target in azimuth and range but are centered on the horizon (this often happens in practice). It is desired that an estimate of the target elevation angle be made so as to generate elevation tracking signals. A single monopulse radar (see Figure 15) will have two signals, U_{mn} and L_{mn}, derived from the

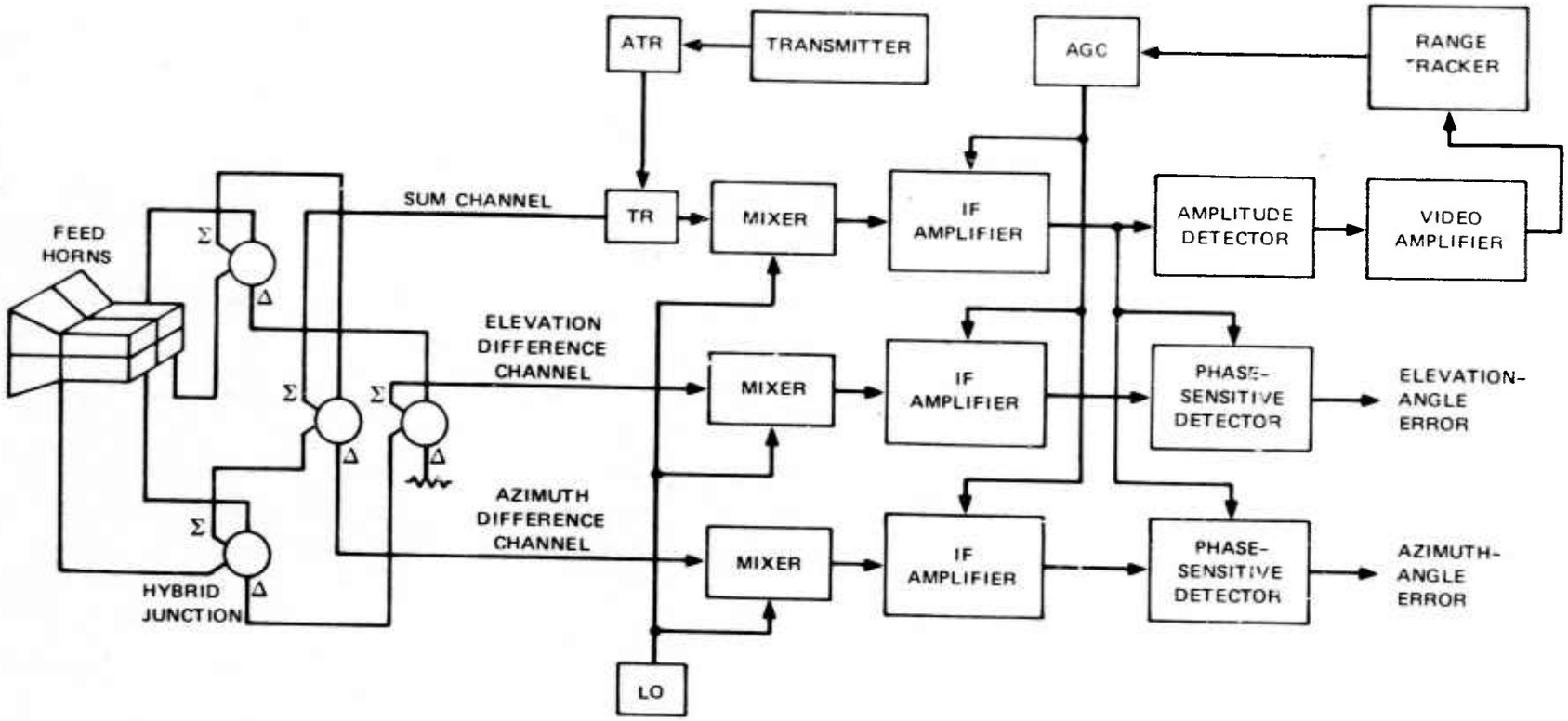

FIGURE 15 BLOCK DIAGRAM OF A CONVENTIONAL MONOPULSE TRACKING RADAR. Source: Skolnik (1970, p. 21-13)

upper and lower horns, respectively. Let $\Delta\theta$ be the true target elevation angle above the horizon (and hence above the radar antenna boresite). Now if we assume that the antenna patterns are linear functions of elevation angle over $\Delta\theta$, then the direct return received by the upper horn is

$$(1 + \Delta\theta) \frac{\psi_{mn}}{r_{mn}^2} e^{j(\omega_n t - k[2r_{mn} - (\epsilon\Delta\theta/2)])}$$

where $(1 + \Delta\theta)$ is the antenna pattern magnitude and $e^{-jk\epsilon\Delta\theta/2}$ is the pattern phase relative to boresight. Thus the response of the upper and lower horns to both the direct and reflected signals can be written as

$$U_{mn} = (1 + \Delta\theta)\left(\frac{\psi_{mn}}{r_{mn}^2}\right) e^{j(\omega t - k[2r_{mn} - (\epsilon\Delta\theta/2)])}$$

$$+ (1 - \Delta\theta)\left(\frac{\Phi_{mn}}{r_{mn}^2}\right) \rho_n e^{j(\omega t - k[2r_{mn} + (\epsilon\Delta\theta/2) + \delta_n])} \qquad (44)$$

$$L_{mn} = (1 - \Delta\theta)\left(\frac{\psi_{mn}}{r_{mn}^2}\right) e^{j(\omega t - k[2r_{mn} + (\epsilon\Delta\theta/2)])}$$

$$+ (1 + \Delta\theta)\left(\frac{\Phi_{mn}}{r_{mn}^2}\right) \rho_n e^{j(\omega t - k[2r_{mn} - (\epsilon\Delta\theta/2) + \delta_n])} \quad . \qquad (45)$$

Now let

$$S_{mn} = \left(\frac{r_{mn}^2}{\psi_{mn}}\right) e^{j(\omega t - 2kr_{mn})} [U_{mn} + L_{mn}] \tag{46}$$

$$D_{mn} = \left(\frac{r_{mn}^2}{\psi_{mn}}\right) e^{j(\omega t - 2kr_{mn})} [U_{mn} - L_{mn}] \quad . \tag{47}$$

Let

$$\beta_{mn} = \Phi_{mn} \rho_n / \psi_{mn} \tag{48}$$

and then

$$S'_{mn} = (1 + \Delta\theta_{mn}) e^{+jk\epsilon\Delta\theta/2} + \beta_{mn}(1 - \Delta\theta) e^{-jk[\delta_n + (\epsilon\Delta\theta/2)]}$$

$$+ (1 - \Delta\theta) e^{-jk\epsilon\Delta\theta/2} + \beta_{mn}(1 + \Delta\theta) e^{-jk(\delta_n - \epsilon\Delta\theta/2)} \tag{49}$$

$$D'_{mn} = (1 + \Delta\theta) e^{jk\epsilon\Delta\theta/2} + \beta_{mn}(1 - \Delta\theta) e^{-jk\epsilon\Delta\theta/2} e^{-jk\delta_n}$$

$$- (1 - \Delta\theta) e^{-jk\epsilon\Delta\sigma/2} - \beta_{mn}(1 + \Delta\theta) e^{+jk\epsilon\Delta\theta/2} e^{-jk\delta_n} \tag{50}$$

Thus, if $\phi = k\epsilon\Delta\theta/2$ and $\eta = k\delta$, and the subscripts m, n are understood, then

$$S' = (1 + \Delta\theta) e^{j\phi} + \beta e^{j\eta}(1 - \Delta\theta) e^{-j\phi} + (1 - \Delta\theta) e^{-j\phi}$$

$$+ \beta\, e^{-j\eta}(1 + \Delta\theta) e^{+j\phi} \tag{51}$$

$$D' = (1 + \Delta\theta)e^{j\phi} + \beta e^{j\eta}(1 - \Delta\theta)e^{-j\phi} - (1 - \Delta\theta)e^{-j\phi}$$

$$- \beta e^{-j\eta}(1 + \Delta\theta)e^{+j\phi} \tag{52}$$

and

$$S' = (e^{j\phi} + e^{-j\phi}) + \Delta\theta(e^{j\phi} - e^{-j\phi})$$

$$+ [(e^{j\phi} + e^{-j\phi}) + \Delta\theta(e^{j\phi} - e^{-j\phi})]\beta e^{j\eta} \tag{53}$$

$$D' = (e^{j\phi} - e^{-j\phi}) + \Delta\theta(e^{j\phi} + e^{-j\phi})$$

$$- [(e^{j\phi} - e^{-j\phi}) + \Delta\theta(e^{j\phi} + e^{-j\phi})]\beta e^{j\eta} \tag{54}$$

or

$$S' = [(e^{j\phi} + e^{-j\phi}) + \Delta\theta(e^{j\phi} - e^{-j\phi})][1 + \beta e^{j\eta}]$$

$$= 2\left\{[\cos\phi + j\Delta\theta \sin\phi][1 + \beta e^{j\eta}]\right\} \tag{55}$$

$$D' = [(e^{j\phi} - e^{-j\phi}) + \Delta\theta(e^{j\phi} + e^{-j\phi})][1 - \beta e^{j\eta}]$$

$$= 2\left\{[j \sin\phi + \Delta\theta \cos\phi][1 - \beta e^{j\eta}]\right\} \quad . \tag{56}$$

Thus,

$$\frac{D'}{S'} = \frac{j \sin\phi + \Delta\theta \cos\phi}{\cos\phi + j\Delta\theta \sin\phi}\left[\frac{1 - \beta e^{j\eta}}{1 + \beta e^{j\eta}}\right] \quad . \tag{57}$$

If $k\ell/2 \gg 1$ and $\phi \gg \Delta\theta$ (and since $\sin\phi \gg \Delta\theta \cos\phi$), we have a phase-comparison monopulse system. The estimate of $\Delta\theta$ made by this system is $\widetilde{\Delta\theta}$ given by

$$\widetilde{\Delta\theta} = \frac{D'}{jS'} \cong \frac{\sin\phi}{\cos\phi}\left[\frac{1 - \beta e^{j\eta}}{1 + \beta e^{j\eta}}\right] = \tan\phi\left[\frac{1 - \beta e^{j\eta}}{1 + \beta e^{j\eta}}\right]$$

$$\cong \Delta\theta\,\frac{k\epsilon}{2}\left[\frac{1 - \beta e^{j\eta}}{1 + \beta e^{j\eta}}\right] \quad . \tag{58}$$

If $k\epsilon/2 \ll 1$, then an amplitude-comparison monopulse system results, and

$$\widetilde{\Delta\theta} = \frac{D'}{S'} = \Delta\theta\left[\frac{1 - \beta e^{j\eta}}{1 + \beta e^{j\eta}}\right] \quad . \tag{59}$$

In either case, if a strong reflection occurs, then $\psi \approx \rho\phi$ and thus $\beta \cong 1$. As η varies over 0 to 2π, $\widetilde{\Delta\theta}$ changes from 0 to infinity. This is the essence of the low-angle tracking problem.

The netting process, a simple average of the sum and difference signals, results in the estimate of the elevation angle $\widetilde{\Delta\theta}$ as given by

$$\widetilde{\Delta\theta} = \frac{\bar{D}'}{\bar{S}'} = \frac{\sum_{m,n=1}^{M,N} D'_{mn}}{\sum_{m,n=1}^{M,N} S'_{mn}} \cong \Delta\theta\,\frac{MN - \sum_{m,n=1}^{M,N} \beta_{mn} e^{j\eta_n}}{MN + \sum_{m,n=1}^{M,N} \beta_{mn} e^{j\eta_n}} \quad . \tag{60}$$

Let

$$\gamma = \frac{1}{MN} \sum_{m,n=1}^{M,N} \beta_{mn} e^{j\eta_n} \quad . \tag{61}$$

Then

$$\widetilde{\Delta\theta} = \frac{\bar{D}'}{\bar{S}'} = \Delta\theta\,\frac{1 - \gamma}{1 + \gamma} \quad . \tag{62}$$

In the case of a single radar system (M = N = 1), it is common to find $\Phi\rho \approx \Psi$ and hence $\beta \approx 1$. Therefore, as η changes, $\widetilde{\Delta\theta}$ varies from near zero for $\eta = 0$ to a very large value when $\eta = \pi$ and the denominator in the equation above approaches zero. So for a single radar, low-angle tracking is often impossible.

Now if three radar sites are netted, the β_{mn} terms add incoherently so that $\sum_{mn} \beta_{mn} e^{i\eta_n}$ approaches zero. The result of summing the β terms is to significantly reduce the variance of $\widetilde{\Delta\theta}$ as more β terms are summed. The result for three sites and hence nine paths is that the variance of $\widetilde{\Delta\theta}$ is reduced from something like $\widetilde{\Delta\theta}$ to a few percent of $\widetilde{\Delta\theta}$. This will produce an impressive enhancement of low-angle tracking performance.

Accurate estimates of the enhancement could be made if probability density functions could be determined for ρ_n, the terrain small-angle reflection coefficient. As mentioned in Section II above, scattering theory and experimental measurements are generally lacking at the low scattering angles of interest. However, Rice (1951) has pointed out that the reflection coefficients (ρ) measured during the survey for the transcontinental microwave relay system could be represented by a Rayleigh distribution having a median value of about 0.28. The grazing angles at the specular reflection point were generally less than one-half degree. An optimal scheme for netting radar sites should produce some improvement over the simple scheme presented here.

If each radar site employs one or more of the other low-altitude improvement techniques discussed in this report, even further improvements can result from netting radar sites together. Moving-target-indicator (MTI) clutter rejection is not degraded by netting and can in fact be similarly enhanced if desired.

c. Passive Radar Receiver Sites

Some of the advantages of multistatic operation have been covered above. The remaining consideration of multistatic operation is best explained by examining the placement of a very simple, passive, nontracking site well ahead of the active tracking radar. Such a scheme is illustrated in Figure 16. Simple time of arrival (TOA) of the direct return from the target and the target return as received by an omnidirectional and passive receiver can then be used to determine altitude without the need to derive vertical tracking-error signals from the active radar-site signals. Doppler filtering can be used to remove clutter in the usual manner. Several such passive receivers might be used around a single active site in order to obtain extensive area coverage of low-altitude targets. The passive sites could be very inexpensive and completely unobservable to incoming aircraft.

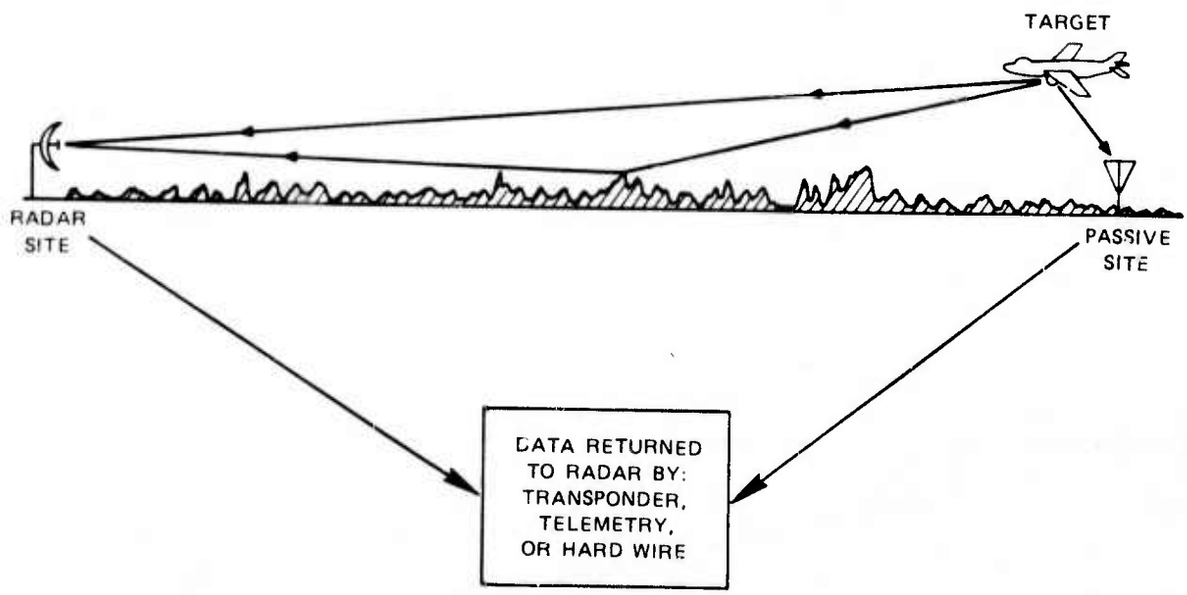

FIGURE 16 RADAR SYSTEM USING AN ADDITIONAL ANTENNA (BISTATIC). The range and azimuth of the target are known sufficiently well. The elevation is determined by the time of arrival of the radar pulse at the passive site. Several such sites could be used to obtain a system that is simple, passive, and inexpensive.

The effectiveness of such a system can be derived by considering the complexity of the calculations needed to determine low-level target altitude and by determining the area coverage of a single passive site.

The target altitude h_t is easily derived from the following known quantities: the target range (R_T), the passive site range (R_S), the difference in azimuth angles to the target and to the passive site (ϕ), and the range between the target and the passive receiver site (r). Figure 17 illustrates the geometry of the situation for which the following equations apply:

$$R_T^2 = R_X^2 + h_t^2 \tag{63}$$

$$r^2 = Z^2 + h_t^2 \tag{64}$$

$$Z^2 = R_X^2 + R_S^2 - 2R_S R_X \cos \phi \quad . \tag{65}$$

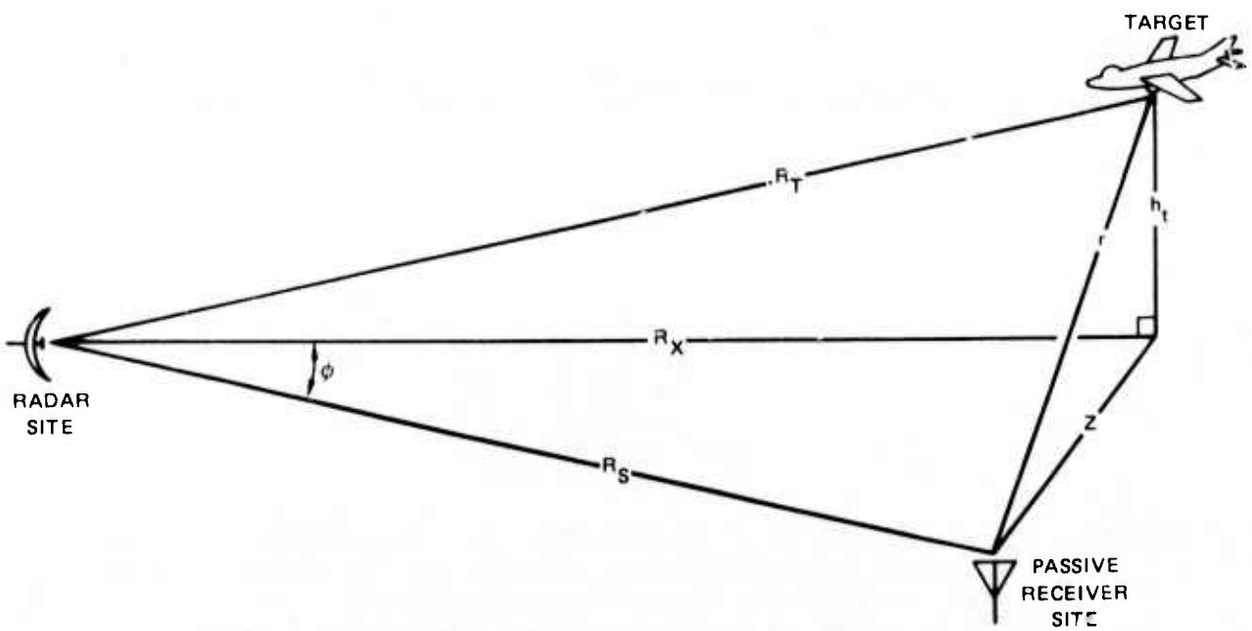

FIGURE 17 GEOMETRY OF THE PASSIVE-RECEIVER SYSTEM

Thus,

$$r^2 - h_t^2 = R_X^2 + R_S^2 - 2R_S R_X \cos \phi \tag{66}$$

and

$$R_X^2 = R_T^2 - h_t^2 \tag{67}$$

or

$$r^2 - h_t^2 = R_T^2 - h_t^2 + R_S^2 - 2R_S\sqrt{R_T^2 - h_t^2} \cos \phi \tag{68}$$

$$r^2 - R_S^2 - R_T^2 = - 2R_S \sqrt{R_T^2 - h_t^2} \cos \phi \tag{69}$$

$$h_t^2 - R_T^2 = \frac{\left(r^2 - R_S^2 - R_T^2\right)^2}{- 4R_S^2 \cos^2 \phi} \tag{70}$$

$$h_t^2 = R_T^2 - \frac{\left(r^2 - R_S^2 - R_T^2\right)^2}{4R_S^2 \cos^2 \phi} \tag{71}$$

$$h_t = \left[R_T^2 - \frac{\left(r^2 - R_S^2 - R_T^2\right)^2}{4R_S^2 \cos^2 \phi}\right]^{\frac{1}{2}} \tag{72}$$

d. Frequency Agility

The ability to dynamically change the radar frequency of operation can be a great aid in low-angle tracking. Barton (1974) gives an excellent detailed discussion of this technique both for frequency hopping and spread spectrum when signal averaging is used, and only a brief additional discussion of another method will be presented here. The usual low-angle tracking problem is encountered when the difference in range between the target and its image is so small that Doppler filtering and range gating cannot affect target separation. If a frequency change Δf in the transmitter frequency is made, then the relative phase angle between the target and its image will change by $2\pi\Delta f\delta/c$ radians where δ/c is the range difference in time (on the order of 0.1 ns). Thus, an extremely wideband radar ($\Delta f > 1$ GHz) could separate the target and image signals by appropriate frequency changes, depending on the received-signal-to-noise ratio. These dynamic frequency-shifting techniques are closely related to the spread-spectrum techniques, but may be considerably easier to implement for equivalent results, especially if only accurate tracking, as opposed to area scanning, is desired.

One method to accomplish this would be to recursively estimate the target range, altitude, and reflected-signal phase, and from this estimate, the altitude difference between the target and image. Then the next probing frequency is selected to change the relative phase so as to alternately maximize and minimize the antenna signal. Altitude information is thus not derived from the antenna position (which centers on the horizon) but from the difference frequency, the range measurement, and the known geometry of the site.

e. Multiple-Antenna Arrays

Multiple antennas provide multiple sources of information about the incoming radar echo and hence may be used to implement the netting and generalized monopulse schemes discussed in Sections III-B-2-a and III-B-2-b above. Multiple antennas may be used in a way very similar to the use of frequency agility, which is examined in Section III-B-2-d above. They may also be used to increase the effective antenna aperture as shown in Section III-B-1-a above. Whether or not additional antennas can provide the most efficient means of implementing these schemes is a question of engineering tradeoffs and will not be considered here. Our purpose is simply to show possible options.

In the case of netting by using multiple antennas at the same site it is necessary to show that the antennas used sample sufficiently different reflected echo signals. As an example, consider antennas displaced vertically at the same site--i.e., having different values of h_r in Figure 2. For the netting scheme (Section III-B-2-b) the estimate ($\widetilde{\Delta\theta}$) of the true elevation angle $\Delta\theta$ is given by

$$\widetilde{\Delta\theta} = \Delta\theta \frac{MN - \sum_{m,n=1}^{M,N} \beta_{mn} e^{j\eta_n}}{MN + \sum_{m,n=1}^{M,N} \beta_{mn} e^{j\eta_n}} \tag{73}$$

For the scheme to work, the values of η_n must be different enough that the $\beta_{mn}e^{j\eta_n}$ terms add incoherently and thus tend to cancel out. Now $\eta_n = k\delta_n$, where $k = 2\pi/\lambda$, and δ_n is the path difference between the direct

signal and the reflected signal to the n^{th} receiving antenna. The question then is, does δ_n vary sufficiently rapidly with changes in receiving-antenna height (h_r)? The approximate expression for δ is given by Kerr et al. (1951, p. 415) as $\delta \approx 2h_t h_r/G$ using the geometry of Figure 6. The phase difference between direct and reflected echoes is $\eta = 2\pi\delta/\lambda$, so the rate of change of η with respect to receiver antenna height (h_r) is $d\eta/dh_r = 4\pi h_t/G\lambda$. Considering the example case h_t = 100 m, G = 10 km, and λ = 3 cm, we find $d\eta/dh_r$ = 4.2 rad phase change per meter change in h_r. For this typical case we see that indeed η_n does change sufficiently rapidly in that a pair of 2-m-diameter dishes placed one right above the other would experience more than an 8-rad phase change between them.

The frequency-agility technique (Section III-B-2-a) separates the reflected radar echo from the direct radar echo by noting that the phase difference between the direct and reflected signals changes by an amount ($2\pi\Delta f\delta/c$) rad when the frequency is changed by Δf. Holding the frequency constant we may also change this phase difference by changing the receiving-antenna height (h_r). The change in phase difference is given by $(d\eta/dh_r)\Delta h_r = (4\pi h_t/G\lambda)\Delta h_r$. For the typical case mentioned above, we have a change in phase difference of 4.2 rad per meter change in h_r. A disadvantage of changing antenna height as opposed to changing frequency is of course that the size of the frequency change Δf can be varied, whereas Δh_r would have only a few discrete values since the multiple antennas would presumably be fixed.

Multiple antennas could very well be used in the formation of multiple antenna beams, as is done with array antennas (Skolnik, 1970, Chapter 11). The resulting multiple beams would then be used with a scattering model as discussed in connection with the generalized signal-processing scheme in Section III-B-2-a.

f. Site Location and Terrain Modification

The elevation error induced by the ground reflection of radar echoes generally increases as the reflection coefficient, ρ, of the surface increases. Hence, one method of improving a radar system's low-angle tracking performance is to reduce ρ by choosing an advantageous site for the radar or physically modifying the terrain in front of the radar, or both. Many radars are portable and can be moved rather easily in order to improve low-altitude performance. It seems likely that the adverse effects of terrain reflection can be reduced by small changes in radar site location. Once a radar site is chosen, it appears likely that modification of a relatively few troublesome spots on the surface can be effective in further reducing ρ. The methods that can be employed to reduce ρ depend strongly on the scattering mechanism responsible for the reflection. So we will consider specular, quasispecular, and diffuse scattering mechanisms separately. Our present understanding of microwave scattering is very inadequate in many situations and at low grazing angles in particular. Therefore a really adequate analysis of the techniques suggested here awaits new advances in low-angle scattering theory and experiments.

The specular scattering mechanism is responsible for the most devastating radar errors because the reflections are phase-coherent and may cancel the direct echo signal completely. The specular point is generally rather close to a low-sited radar, making modifications of the relevant region around the specular point fairly convenient. On the other hand, for low-angle targets the first Fresnel zone, from which most of the specular reflection comes, is rather large. For example, if we assume a plane geometry as in Figure 6, the distance to the specular point X_s is only about 0.5 km from the radar when $h_r = 5$ m, $h_t = 100$ m, and $G = 10$ km.

However for an X-band (λ = 3 cm) radar the first Fresnel zone is an ellipse extending about 2.8 km along the radar's line of sight and about 30 m perpendicular to it. As noted in Section II the specular reflection decreases markedly as the surface becomes more rough. So if we can site the radar such that the first Fresnel-zone region about the specular point is relatively rough, specular reflection will be reduced and low-angle performance aided. If the site is fixed, one could try roughening the surface artificially by plowing or planting appropriate vegetation. Evans (1966) reported that one-foot-high grass reduced the power reflectivity ρ^2 of a particular site by a factor of 16. Another idea tried out by Evans (1966) was to erect an aluminum screen near the specular point to shield the specular-reflection region from the radar. This scheme resulted in a 15-db reduction in ρ^2 for the most favorable elevation angle of the target. As the target moves, of course, the specular point will also move. Even so, a single screen was helpful over a range of elevation angles. Another option, discussed by Smith and Melling (1974), is to have the radar sited high enough that it "looks over" the specular-reflection region.

The quasispecular scattering mechanism assumes that the reflecting surface is broken into a number of small reflecting facets or specular points (Kodis, 1966). These small reflecting regions are randomly tilted with respect to the mean vertical direction like the cracked surface of a boiled egg. Though relatively small, the facets are large compared to the wavelength. For a given geometry, some of these facets will be properly oriented for specular reflection, and it is these facets that provide the scattered wave. Usually one assumes that the probability distribution of facet tilts is Gaussian, so one finds fewer properly aligned facets as one moves away from the specular point. The properly aligned facets near the specular point provide a coherent surface reflection while those further away provide an incoherent reflection component.

As the average tilt of the facets measured by the unidirectional rms slope ($\tan \beta_o$) increases, the incoherent component becomes more important. As with specular reflection above, siting or terrain modification to make the surface near the specular point rough will reduce the coherent component and thus aid low-angle radar performance. Once the region around the specular point is sufficiently rough, one expects that for low-angle scattering there will be a relatively small number of properly aligned facets here and there. If these troublesome facets could be located and modified either by earth moving, vegetation cover, or possibly conducting screens, then ρ would be reduced still further, with a resulting improvement in radar performance. Of course the specular point and troublesome facets will change with target range and elevation; but as with the shielding screens mentioned above, it is expected that improvements can be effected over a range of target parameters. Virtually no closely relevant experimental data have yet come to light, and this is just what is needed to determine how practical these schemes are. However, Bullington (1954) notes that the horizontal movement of an antenna by only 100 ft reduced the low-angle reflection coefficient ρ from 0.72 to 0.55. Some experimental suggestions are made in Section IV.

The diffuse-scattering mechanism provides an incoherent reflection from virtually the entire scattering surface. This mechanism is not well understood, but is apparently due to roughness on a scale small compared to the wavelength--e.g., from small rocks and debris on the scattering surface. Diffuse scattering is very broad and not strongly concentrated in the specular direction as are the specular and quasispecular scattering. Hence, the $(1/r_1 r_2)$ term in Eq. (2) is important, and diffuse scattering will probably arise mainly in foreground (near the radar) and horizon (near the target) components. So, to reduce diffuse

scattering, particular attention should be paid to the foreground component. Siting the radar so as to "look over" the foreground component will be helpful. Possibly a layer of vegetation over the surface rocks and debris would reduce diffuse scattering. Here again, relevant theoretical and experimental work are virtually nonexistent and a critical evaluation of the role of diffuse scattering in low-angle radar performance awaits new developments.

Once one finds that the reduction of the surface reflection coefficient is a practical possibility for a given situation, then one wants to know just how much low-angle tracking performance is improved for a given reduction in ρ. This calculation is rather involved and depends mainly on the following parameters: radar-target geometry, target elevation relative to the horizon θ_t, data processing used at the radar (e.g., whether or not data smoothing is used), radar antenna beam patterns (sum and difference), and surface scattering model.

Barton (1974, pp. 695-698) has looked into this problem and evaluated the expected angular error for various values of the aforementioned parameters. For a standard monopulse radar he finds that the transition from stable to unstable tracking occurs when the target elevation angle θ_t (see Figure 11) is between 0.1 and 0.7 antenna beamwidths (θ_e), depending on the radar-target geometry, the surface scattering model and the radar data-processing algorithm. Whenever $\rho > 0.7$ and $\theta_t < 0.7\ \theta_e$, there will be a strong tendency for the radar to track a false position near the horizon, which is approximately midway between the real target and its image (see Figure 1).

It is difficult to generalize, since so many parameters are involved. However, the following example taken from Barton (1974)

is instructive in showing the sort of improvement one can expect. Consider a target at 10 km range being tracked by a standard monopulse radar at a height of 5 m and with an antenna beamwidth θ_e = 20 mrad. The rms elevation error (σ_E) rises as the target position approaches the horizon--i.e. as θ_t approaches zero. Let us use the value of θ_t (let us call it θ'_t) at which the error σ_E equals 0.2 θ_e as a figure of merit--the smaller θ'_t, the better the low-angle performance. Barton analyzes three types of scattering surface: a smooth surface with rms height deviation h = 5 cm, a medium surface with h = 25 cm, and a rough surface with h = 1 m. The values of θ'_t for these smooth, medium, and rough surfaces are 15, 11, and 3 mrad, respectively. From this analysis it is clear that substantial gains in low-angle radar performance can be obtained by reducing the surface reflection coefficient, especially near the specular point.

All the above discussion has been directed toward reducing ρ. There may well be occasions when a particular reflecting facet in the horizon region could be used along the lines of the small transponders discussed in Section III-B-2-c above.

g. Multiple Radar Fences

One form of specialized terrain modification is the implanting of radar fences to block the return signals reflected from the terrain. Some benefits could result from the proper placement and adjustment of multiple fences near the radar site. The important considerations for a single fence are reviewed by Barton (1974), but additional benefits from multiple fences were not considered. In a crude way of thinking, multiple fences effectively increase the antenna aperture so that the main antenna lobe is narrowed near the horizon enough to discriminate between the direct target and the reflected returns.

Clutter fences are commonly used to reduce backscatter from the nearby ground. In certain types of terrain they can also be used to block below-the-horizon signals. Such a technique has been discussed by Hey and Parsons (1955). The fences can be placed to create an artificial horizon, below which signals will be strongly attenuated as shown in Figure 18. The major disadvantage of the multifence horizon is that it is necessarily flat, and in uneven terrain it may be possible for a target aircraft to fly below it and be lost.

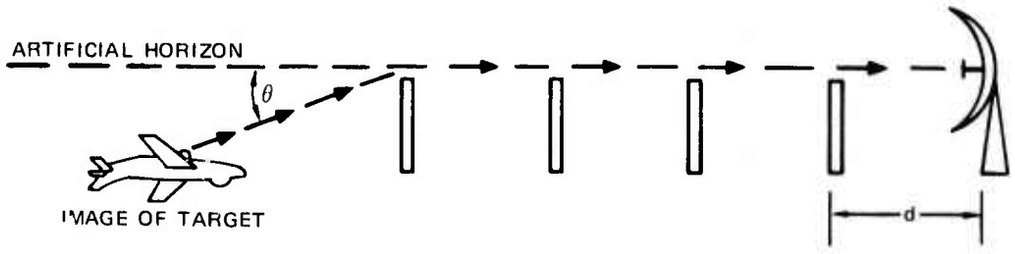

FIGURE 18 ARTIFICAL HORIZON CREATED BY MULTIPLE RADAR FENCES. The angle θ is negative below the artificial horizon and positive above. The image of the target in the ground is suppressed by the screens.

In order to get a crude estimate of the effect of such a row of fences, we shall use an optical approximation, in which each fence is assumed to be in the far field of the preceding fence. Let the distance from the target to the first fence by D, and the distance between the first fence and the radar dish be d. Typically, we may have D = 10 km and d = 100 m. For the scattering off the fence nearest the target, we can assume that the reflected signal from the target is a plane wave (since $D \gg d$). The scattered intensity is given by the Fresnel integrals as illustrated in Figure 19 (see Born and Wolf, 1975, pp. 433-434).

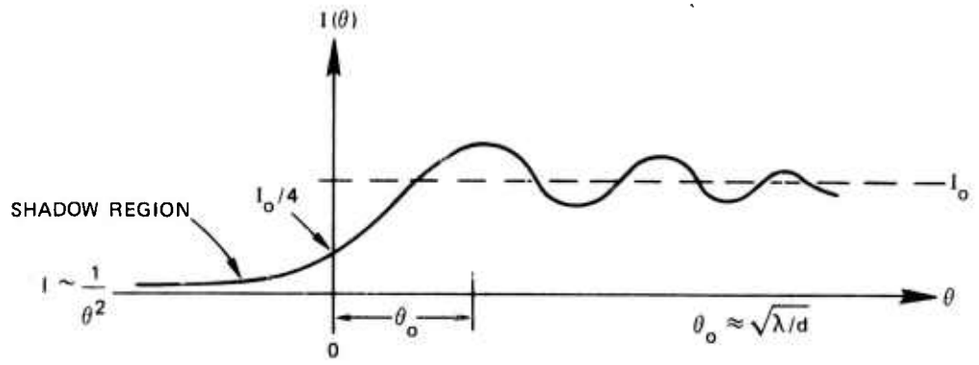

FIGURE 19 SCATTERED INTENSITY AS A FUNCTION OF ANGLE θ ABOVE ($\theta > 0$) AND BELOW ($\theta < 0$) A SINGLE KNIFE EDGE LOCATED AT $\theta = 0$

For the sake of illustration, take $\lambda = 3$ cm, and let the diameter of the dish be $A = 2$ m. Then the characteristic fence attenuation angle $\theta_o \approx \sqrt{\lambda}/d = 1^\circ$ is comparable to the main-lobe width of the dish, $\theta_d = (1.22\lambda)/A = 1^\circ$. The main lobe will be reduced slightly on the ground side, and the lower sidelobes will be replaced by a $1/\theta^2$ monotonic fall-off. For longer wavelengths, the effect of the fences on the main lobe becomes more significant.

The added effect of the additional fences is difficult to estimate, but a crude guess would be that the below-the-horizon signal is reduced by $(\frac{1}{4})^N$, where N is the number of fences in addition to the outermost fence.

Although the below-the-horizon signal is reduced, the fences may introduce a new error for above-the-horizon signals due to the oscillations of the intensity of refracted signal. This error can be reduced in several ways:

(1) The multiple fences can be spaced in such a way that the oscillations from the separate fences tend to cancel.

(2) The top of the fence can be saw-toothed; this should have the effect of "apodizing" the aperture and eliminating the high-spatial-frequency oscillations.

(3) The analysis system can be preprogrammed to compensate for the well known effect that the fences will have on any particular radar system.

A more precise analysis of a multifence system will require either a more detailed mathematical calculation or a computer simulation. A final evaluation will not be possible until such work is completed.

h. Use of Azimuth Information

The scattering of a radar return by a rough surface occurs in both the elevation and azimuth directions. Rough terrain also has appreciable correlation lengths in both directions, so that the scattering in azimuth should exhibit some correlation with scattering in elevation (see Figure 20). This phenomenon cannot be used alone to improve low-altitude tracking; but if the generalized monopulse technique discussed in Section III-B-2-a above is employed, then nonspecular reflections can become the major difficulty and information derived from the azimuth tracking circuits can be used to estimate and hence compensate for the diffuse reflections. A good theory of radar scattering processes would be very useful in quantifying the utility of these signals.

i. System Optimization Using State-Space Modeling

All the techniques discussed in this section have uncertainties, and difficulties develop for weak returns and extremely low elevation angles. Thus it is easy to argue that an optimum combination of several of the techniques can overcome (or at least improve) some of the limitations of any given technique. This could be accomplished in

practice by formulating the known range of target parameters, the radar characteristics, etc. into a state-space model suitable for optimal recursive estimation of the target altitude as a function of all received signal information. The block diagram of such a model is shown in Figure 21. This would be a difficult task, both in the initial formulation for a given radar configuration and in the real-time calculations required to perform the Kalman filtering, but it could have a very significant impact on radar performance. [For reference, Kalman filter is discussed by Schwartz and Shaw (1975)]. If an existing radar network were to be upgraded in capability, this additional signal processing might be a very attractive alternative to other major changes in the radar system.

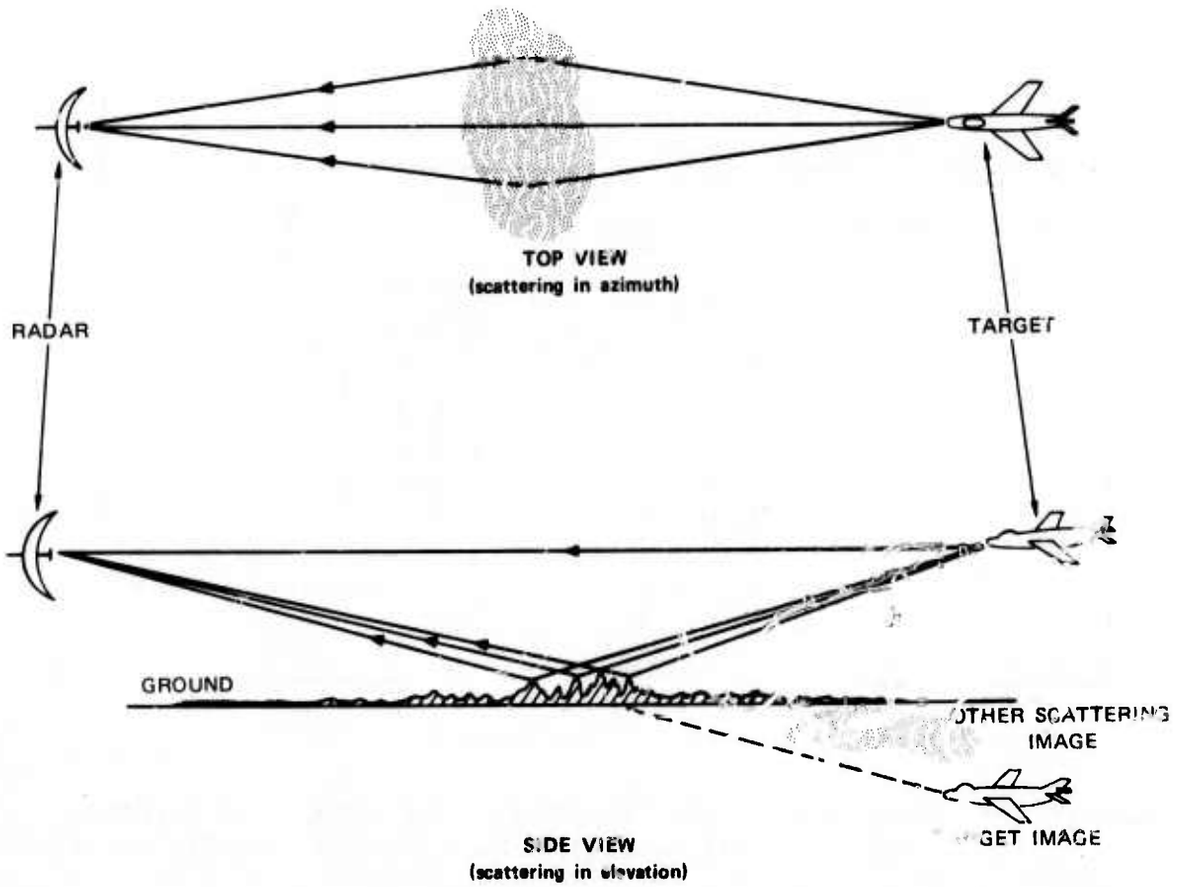

FIGURE 20 CORRELATION BETWEEN SCATTERING IN AZIMUTH (top view) AND SCATTERING IN ELEVATION (side view)

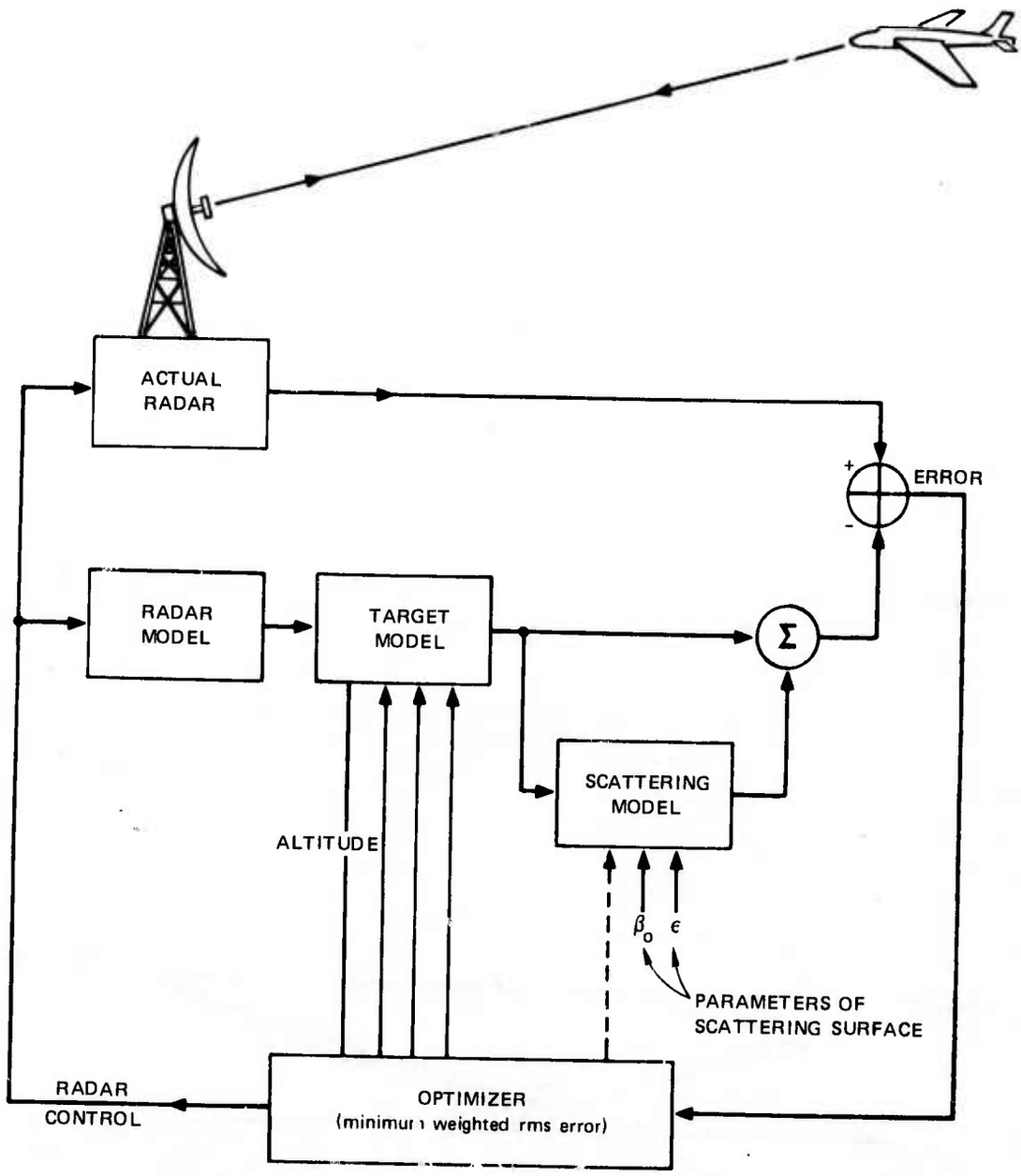

FIGURE 21 GENERAL MODEL OF RADAR SYSTEM SUITABLE FOR OPTIMAL RECURSIVE ESTIMATION OF TARGET PARAMETERS SUCH AS HEIGHT, RANGE, AND AZIMUTH

IV CONCLUSIONS AND RECOMMENDATIONS

A. Scattering Theory

1. Present Deficiencies in Scattering Theory Relevant to Low-Angle Radar Tracking

If scattering laws for a particular range of parameters are well understood, one can predict with confidence how the direct and reflected radar echoes will differ, and algorithms to do the discrimination (see Section III) can be evaluated. Understanding of the scattering laws may also suggest discrimination algorithms. At present there are many deficiencies in scattering theory that manifest themselves as uncertainties in the predicted low-angle tracking errors for a given radar system. The 1960s saw considerable advances in the theory of electromagnetic wave scattering from statistically rough surfaces. This relatively rapid advance slowed around 1970, by which time the quasispecular theory had been developed and had satisfactorily explained a good deal of experimental data. However, important deficiencies in this and other theories remain, as noted in the following paragraphs.

Quasispecular theory breaks down at low grazing angles because shadowing of one part of the surface by another and multiple scattering have been neglected. Shadowing theories exist, but remain largely untested by comparison with experiment. A brief comparison of a particular shadowing theory with relevant lunar bistatic radar data is made in Section II above. Clearly the inclusion of shadowing is helpful, but a comprehensive comparison remains to be done. No treatment of multiple scattering, which is particularly relevant at low grazing angles, has yet come to the authors' attention.

Diffuse scattering is thought to arise mainly from surface roughness on scales small compared to the wavelength. At present no really good statistical or geometric theory exists for the diffuse component for any grazing angle. The semi-empirical Lambertian and Lommel-Seeliger scattering laws [Eqs. (13) and (14)] are the only ones available. To date no comparison of these laws or any other diffuse theory appears to have been made with experimental data at low grazing angles.

Scattering from vegetation is obviously a difficult problem, especially at low grazing angles. According to Barrick (1970), the model of Peake (1959a and 1959b) is the only model that can describe scattering from vegetation-covered surfaces. However, Peake's model does not agree well with experimental backscatter measurements at low grazing angles. So, for the case of special interest here, we must conclude that no good scattering law for vegetation exists.

2. Recommendations for Further Work

The 100-page chapter on rough surface scattering by Barrick (1970) in the ARPA-sponsored Radar Cross Section Handbook was very useful in the present study. It discussed and evaluated existing rough-surface scattering theory up to 1970 and compared theory with experimental results for backscatter. It is recommended that a similar effort again be sponsored by ARPA to include work since 1970, with an emphasis on forward scatter at low grazing angles. Such an effort would provide an evaluated collection of existing theories that could be used to make interim evaluations of radar systems, pending advances in scattering theory. It would also provide a good jumping-off point for new theoretical work. The substantial research results in the Soviet literature should not be neglected. A Russian book on wave scattering from a

statistically rough surface by Bass and Fuchs (1972) is now being translated and edited by C. B. Vesecky and J. F. Vesecky and will be published by Pergamon Press in early 1976.

The deficiencies in scattering theory mentioned above still remain, in part because of the inherent difficulty of the low-angle scattering problem and in part because a great deal of data--for example, in radar astronomy--can be interpreted successfully without worrying about the angles near grazing incidence. Therefore, it is recommended that ARPA sponsor theoretical research work to remedy these deficiencies at low grazing angles. There are probably many approximations that one can exploit at near grazing incidence, but that are invalid elsewhere. Therefore, an ARPA program could well benefit from emphasizing the development of scattering theory that may be valid only at near grazing incidence, in contrast to work that attempts to solve scattering problems for all angles of incidence. Quasispecular scattering, diffuse scattering, and scattering from vegetation all demand attention equally, though it might be possible to order priorities if a specific scattering terrain were known to be of special interest. Close contact should be maintained between those doing theoretical work and those doing the scattering experiments recommended below.

B. Scattering Experiments

1. Microwave Experiments

We can classify microwave experiments into two broad categories. First, there are experiments that are designed to be critical tests of scattering theory, and it is these that are of most interest here. Second, there are experiments designed to establish empirical scattering laws for specific conditions. There are a number of inherent problems in comparing theory with available experimental data, and it is best to

mention these problems in the hope that future experiments will seek to avoid them. First, experimental results are often quoted in terms of the power reflection coefficient (ρ^2) for a particular set of experimental conditions. While ρ^2 is a very useful quantity in practice, it is not an ideal point of comparison between theory and experiment. Since ρ^2 is an integral quantity often summing up contributions from large portions of the scattering surface, agreement between theory and experiment on one or several values of ρ^2 could happen by chance and cannot be taken as confirmation of a theory. Experiments should note the variation of ρ^2 over a wide range of experimental parameters, such as grazing angle and rms surface slope.

Another difficulty arises in the measurement of the scattered radiation. A full specification of the scattered wave requires the measurement of the general Stokes parameters as a function of direction and time of arrival as well as Doppler shift. While experimental measurement of a full specification is a substantial task, it may be necessary in order to make crucial comparisons of theory with experiment.

A genuine test of theory by experiment must also include a sufficiently accurate characterization of the scattering surface. For example, quasispecular theory requires measurement of the unidirectional rms surface slope on a scale larger than the wavelength λ. Diffuse scattering theory would probably be related to surface variations on scales less than λ. So surface characteristics need to be measured on scales varying from much smaller to much larger than λ. Often the scattering surface during an experimental run is so poorly known in some respects that the resulting data cannot be compared with theory. It is best to choose a scattering surface that is not overly complex, since even relatively simple surfaces are not well understood at low grazing angles.

Designing a good experiment that allows a crucial comparison with theory will not be an easy task. The following is a summary of some of the tasks that need to be accomplished:

(1) Identify key assumptions of a theory and design experiments to find out when these assumptions break down.

(2) Design experimental conditions so that the radiation scattered by different scattering mechanisms may be separated.

(3) Measure a sufficiently full specification of the scattered wave, including the full set of general Stokes parameters if necessary.

(4) Measure a sufficiently full set of scattering-surface parameters over the necessary scale lengths, which may be both much longer and much shorter than the wavelength.

If we are to understand rough surface scattering at low grazing angles, it will be necessary to conduct experimental work to help remedy the deficiencies in scattering theory noted above. It is therefore recommended that three types of experiments be carried out, as described below.

a. Vegetation Scattering Experiments

This type of experiment would initially be directed toward testing the Peake (1959a and 1959b) geometric scattering theory. At first, vegetation duplicating Peake's model as closely as possible should be used as a scattering surface--i.e., vegetation resembling the dielectric rods randomly distributed, but preferring the vertical, and having their upper ends terminated on a horizontal plane. Microwave scattering at all angles of incidence would be explored, but with a heavy emphasis on grazing incidence. The full set of general Stokes parameters of the scattered wave would be measured for a variety of

incident polarizations. The experimental objective would be to find when and why the model breaks down by varying the experimental conditions, one parameter at a time, until theory and experimental measurements diverge.

b. Quasispecular Scattering Experiments

Quasispecular theory tends to break down for directions away from the specular direction and for grazing incidence. The experimental objective would again be to find just when and, if possible, why the model breaks down, by varying experimental conditions. The scattering surface should conform as closely as possible to the gently undulating surface assumed in the theory. The full Stokes parameters of the scattered wave should be measured in order to separate out the quasispecularly scattered radiation, as done by Tyler and Howard (1973). For angles near grazing incidence, the shadowing theory of Bass and Fuchs (1972) (see Section II) should be used to modify the quasispecular cross section of Eq. (II-4).

Another interesting quasispecular scattering experiment involves a CW transmitter flown at low altitude over the scattering surface. Such an experiment using the Apollo command module as a transmitter and an Earth-based receiver observing waves scattered off the lunar surface is described in Section II. A more detailed comparison of quasispecular theory including shadowing with this lunar bistatic data (along the lines of the work in Section II) would be a useful test of quasispecular theory, including shadowing near grazing incidence. Another option would be to perform a similar experiment with a CW transmitter flown at low altitude over the Earth's surface. Such an experiment would in principle allow one to find the number and location of the "specular points" responsible for the quasispecularly scattered signal, and hence an opportunity to try out the terrain modification scheme suggested in Section III.

c. Diffuse Scattering Experiments

At present there appears to be no really useful diffuse scattering theory. However, the semi-empirical Lambertian and Lommel-Seeliger scattering laws [Eqs. (13) and (14)] are often used to model diffuse scattering in the absence of better alternatives. It would be useful to know just how well these laws agree with experimental measurements near grazing incidence and over scattering surfaces of varying roughness. A well-conducted experiment paying particular attention to surface roughness on scales small compared to the wavelength could well be helpful in developing a viable diffuse-scattering theory.

2. Laboratory Experiments

Although one naturally thinks of microwave scattering experiments being done with natural terrain in the field, it may also be helpful to conduct experiments with carefully prepared model surfaces in the laboratory. Near-field and edge effects would complicate laboratory experiments, but since the wavelengths of direct concern here are only a few centimeters at most, it may well be possible to overcome the difficulties. In addition, scaled experiments using shorter wavelengths could help solve these problems--for example, by using millimeter-wave sources and possibly lasers. Laboratory experiments usually provide the advantages of closer control over experimental conditions. Theories based on laboratory experiments would still have to be tested in the natural environment.

C. Radar Systems

1. Data Processing Algorithms

The arguments of Section III-B-2-a demonstrate that many of the difficulties that monopulse radars encounter during low-angle tracking are simply artifacts of the particular data-processing algorithm used.

With appropriate but modest changes in monopulse radar configuration and data-processing algorithms, a radar can successfully track targets at low elevation angles. Practical implementation of a first-order scheme along the same lines as suggested in Section III-B-2-a has been accomplished by White (1974) with very encouraging results, especially over water. It is therefore recommended that a program be initiated to accomplish the following:

(1) Study a variety of radar modifications and data-processing algorithms.

(2) Determine the sensitivity of the above processing algorithms to variations in the surface scattering model and other radar system parameters such as signal-to-noise ratio.

(3) Field experiments that demonstrate the advantages that occur with modified processing.

The theoretical study program, (1) and (2), would be at the 2- to 3-man-year level for one year. A comprehensive theory of radar signal processing relative to multiple-feed antennas, antenna arrays, and radar fences and involving electromagnetic-wave scattering theory is needed. The general approach could begin with the development of optimal algorithms for the estimation of the parameters of the general model presented in Figure 21. Such optimal mathematical programming algorithms have been extensively applied in control theory, but very little work along these lines appears to have been directed toward radar systems and none at all toward the low-angle tracking problem. An important input to the theoretical study of processing algorithms would be the results of the studies of scattering from a rough surface at grazing incidence recommended above.

2. mm-Wave Radars

Low-angle tracking performance can be greatly improved in a straight-forward way by simply reducing the radar antenna beamwidth. Thus, the interfering multipath signal is rejected by the high angular resolution of the radar antenna. In Sections III-B-1-a and III-B-1-b, two methods of achieving sufficient antenna resolution are discussed. The first is simply to use a larger antenna aperture. The second is to use a higher operating frequency. The numerous advantages of small antennas, e.g., dishes of one meter and smaller diameter, tend to make one favor the latter option. With regard to this option it is concluded that operating radars at higher frequencies (K band and mm wavelengths) can greatly improve their low-angle tracking performance by allowing one to obtain very narrow antenna beamwidths with relatively small antennas--the higher the frequency, the greater the improvement. However, as one operates at progressively higher frequencies, progressively higher atmospheric attenuation and receiver noise levels require that the peak transmitter power (P_t) be correspondingly increased. While the required peak transmitter power at 10 mm (K_a band) is within current technological capabilities, P_t rises well above a megawatt at 1.35 mm for a target at 20 km range. Since current transmitter peak powers at around 1 mm fall in the 1-10 watt range, substantial increases in transmitter peak power capability at mm wavelengths are required in order to exploit the superior low-angle tracking performance at these wavelengths. Improvements in receiver system noise temperature over the estimates used in Section III-B-1-b could also be helpful, though such efforts would only reduce the required value of P_t by about a factor of 4. It should also be noted that at short wavelengths (like 1.35 mm) antenna surface tolerances become very tight indeed (~0.05 mm) if satisfactory performance is to be achieved.

The current ARPA program in high power mm wave sources may provide the necessary high power levels at mm wavelength. When mm wave sources in the megawatt range become feasible, research and development of a mm wave low-angle tracking radar should be considered so that the superior performance at mm wavelengths can be speedily exploited. As the characteristics of high power mm wave sources become better known, improvements in mm wave receiver technology should be studied to see if funding in this area would be cost effective in light of the possible benefits to mm radar systems.

Appendix

COMPUTER PROGRAM FOR CALCULATING RADAR PARAMETERS

Appendix

COMPUTER PROGRAM FOR CALCULATING RADAR PARAMETERS

```
BEGIN COMMENT:TEST LOW ALTITUDE RADAR DIFFTIME.BY DESPAIN DEC 74..;
FILE IN(KIND=REMOTE),OUT(KIND=REMOTE);LABEL HELL;
FORMAT DOUBLELINE
("==========================================================================/
      /=");
FORMAT SINGLELINE
("--------------------------------------------------------------------------/
      /-");
REAL R,T,A,RS,RM,TS,TM,AS,AM,FREQ,RMS,GAMMA THETA,APERTURE,C,PI;

REAL PROCEDURE DIFFTIME(RANGE,TARGETHEIGHT,ANTENNAHEIGHT);
 REAL RANGE,TARGETHEIGHT,ANTENNAHEIGHT;  BEGIN
 COMMENT:CALCULATION OF THE TIME DELAY BETWEEN THE DIRECT
         RETURN SIGNAL AND THE REFLECTED SIGNAL FOR LOW
         ALTITUDE RADAR TRACKING.  BY DESPAIN DEC 74.....;
 REAL R,T,A,R2,C,DELTA;C:=299800000;A:=ANTENNAHEIGHT;
 T:=TARGETHEIGHT;R2:=RANGE*RANGE;IF (T+A)=0 THEN DELTA:=0
 ELSE DELTA:=SQRT(R2+(A+T)**2)-SQRT(R2+(A-T)**2);
 DIFFTIME:=DELTA/C;END DIFFTIME;

 REAL PROCEDURE RHO(GAMMA,BETA);REAL GAMMA,BETA;BEGIN
 COMMENT:J. VESECKEY'S BISTATIC SCATTERING FORMULA.BY DESPAIN 74.;
 REAL Q, RHOPRL,RHONML,E,PI,A;
  REAL PROCEDURE LAMBDA(A);REAL A;BEGIN COMMENT: LAMBDA FUNCTION;
  LAMBDA:=(1/2*A)*(SQRT(2/PI)*EXP(-A**2/2)-A*ERFC(A/SQRT(2)));END;
 PI:=0.14159265359;
 E:=3.0;COMMENT: E IS THE SURFACE DIELECTRIC CONSTANT;
  IF BETA NEQ 0 THEN BEGIN
 A:=TAN(GAMMA)/(SQRT(2)*TAN(BETA));
 Q:=(1/(1+2*LAMBDA(A)));END  ELSE Q:=1;
 RHOPRL:=((E*SIN(GAMMA)-SQRT(E-COS(GAMMA)**2))/
          (E*SIN(GAMMA)+SQRT(E-COS(GAMMA)**2)))**2;
 RHONML:=((SIN(GAMMA)-SQRT(E-COS(GAMMA)**2))/
          (SIN(GAMMA)+SQRT(E-COS(GAMMA)**2)))**2;
 RHO:=.5*(RHOPRL+RHONML)*Q;
 END RHO;
```

```
 PI:=3.14159265359;C:=299800000.;
WRITE(OUT,<"ENTER RADAR CENTER FREQUENCY(MHZ)">);      READ(IN,/,FREQ);
WRITE(OUT,<"ENTER RMS SURFACE SLOPE">);                READ(IN,/,RMS);
WRITE(OUT,<"ENTER TARGET HEIGHT STEPS(METERS)">);      READ(IN,/,TS);
WRITE(OUT,<"ENTER MAXIMUM TARGET HEIGHT(METERS)"> );   READ(IN,/,TM);
WRITE(OUT,<"ENTER ANTENNA HEIGHT STEPS(METERS)">);     READ(IN,/,AS);
WRITE(OUT,<"ENTER MAXIMUM ANTENNA HEIGHT(METERS)">);   READ(IN,/,AM);
WRITE(OUT,<"ENTER RANGE STEPS (KILOMETERS)">);         READ(IN,/,RS);
WRITE(OUT,<"ENTER MAXIMUM RANGE(KILOMETERS)">);        READ(IN,/,RM);
 FREQ:=FREQ*1.0@06;RS:=1000*RS;RM:=1000*RM;

WRITE(OUT[SPACE 4]);
WRITE(OUT,<"TESTING THE DIFFTIME AND THE SCATTERING LAW">);
 FOR T:=TS STEP TS UNTIL TM DO BEGIN
 FOR A:=AS STEP AS UNTIL AM DO BEGIN
WRITE(OUT,DOUBLELINE);WRITE(OUT[SPACE4]);
WRITE(OUT,DOUBLELINE);WRITE(OUT,
<X10,"     LOW ALTITUDE RADAR SCATTERING PARAMETERS ">);
WRITE(OUT,SINGLELINE):WRITE(OUT,<X2,
"TARGET HEIGHT =",R6.2," METERS  ,   ANTENNA HEIGHT ="R6.2," METERS"
 >,T,A);
WRITE(OUT,SINGLELINE);WRITE(OUT,<
"   RANGE   TIME DELAY  SCATTER RANGE    ANGLE   AMPLITUDE  APERTURE/
     /">);
 WRITE(OUT,<
" (METERS)  (NANOSECONDS)  (METERS)    (RADIANS)   (RATIO)  (METERS)/
     /">);
WRITE(OUT,SINGLELINE);
FOR R:=R5 STEP RS UNTIL RM DO BEGIN
 IF R=0 THEN GAMMA:=THETA:=1 ELSE BEGIN
 GAMMA:=ARCTAN((A+T)/R);THETA:=ARCTAN((T-A)/R)+GAMMA;END:
 APERTURE:=C/(THETA*FREQ);
 COMMENT:STEGEN FORMULA.REF:JASIK,"ANTENNA HANDBOOK",P2-24;
 WRITE(OUT,<R9.2,R13.6,R12.2,X2,R9.6,X2,R9.6,R11.4 >,
 R,DIFFTIME(R,T,A)*0+9 R*A/(A+T),THETA,RHO(GAMMA,RMS),APERTURE);
END;END;END;
HELL:END TESTDIFFTIME.
```

REFERENCES

Armstrong, D.G., P.E. Cornwell, and A.H. Greene, "Final Technical Report for Multipath Measurements", Contract DAAH01-74-C-0704 (ARPA Order 2731), Raytheon Advanced Development Laboratory, Wayland, MA (1974).

Barrick, D.E., and W.H. Peake, "Scattering from Surfaces with Different Roughness Scales: Analysis and Interpretation", Report BAT-197A-10-3, Battelle Memorial Institute, Columbus Laboratories, Columbus, OH (1967).

Barrick, D.E., "Rough Surfaces", Ch. 9 in Ruck, G.T. et al., Radar Cross Section Handbook, Plenum Press, New York, NY (1970).

Barton, D.K., "Low-Angle Radar Tracking", Proc. IEEE, Vol. 62, p. 687 (June 1974).

Bass, F.G., and M. Fuchs, Wave Scattering on a Statistical Rough Surface (in Russian), Izd-vo "Nauka", Glav. red. fix. - mat. lit-ry, Moscow, 1972. Chapter 22, "Calculation of Shadowing for Reflection from a Statistically Rough Surface", and Chapter 23, "Effective Distribution Functions of Height and Slope when Shadowing is Present", have been translated by C.B. Vesecky. Translation of the entire book by C.B. and J.F. Vesecky is underway for Pergamon Press, with publication scheduled for Spring 1976.

Beard, C.I., "Coherent and Incoherent Scattering of Microwaves from the Ocean", IRE Trans. on Antennas and Propagation, Vol. AP-9, p. 470 (1961).

Beckman, P., and A. Spizzichino, The Scattering of Electromagnetic Waves from Rough Surfaces, Macmillan Co., New York, NY (1963).

Beckman, P., "Shadowing of Random Rough Surfaces", IEEE Trans. on Antennas and Propagation, Vol. AP-13, p. 384 (1965).

Born, M., and E. Wolf, Principles of Optics, Pergamon Press, Oxford, England (1975).

Brockleman, R.A., and Hagfors, "Note on the Effect of Shadowing on the Backscatter of Waves from a Random Rough Surface", IEEE Trans. on Antennas and Propagation, Vol. AP-14, p. 621 (1968).

Buck, G.J., and J.J. Gustincic, "Resolution Limitations of a Finite Aperture", IEEE Trans. on Antennas and Propagation, Vol. AP-15, No. 3, pp. 376-381, (May 1967).

Bullington, K., "Reflection Coefficients of Irregular Terrain", Proc. IRE, Vol. 43, p. 1258 (1954).

Christiansen, W.N., and J.A. Hogbom, Radiotelescopes, Cambridge University Press, Cambridge, England (1969).

Dax, P.R., "Accurate Tracking of Low Elevation Targets over the Sea with a Monopulse Radar", RADAR-Present & Future, IEEE Conference Publication No. 105, London, England (1973).

Evans, G.C., "Influence of Ground Reflections on Radar Target Tracking Accuracy", Proc. IEEE, Vol. 113, p. 1281 (1966).

Evans, J.V., and T. Hagfors, Radar Astronomy, McGraw-Hill Book Co., New York, NY (1968).

Evans, J.V., "Radar Studies of Planetary Surfaces", in Ann. Rev. of Astron. Astrophys. (L. Goldberg, ed.), Vol. 9, Annual Reviews, Inc., Palo Alto, CA (1970).

Fjeldbo, G., "Bistatic-Radar Methods for Planetary Ionospheres and Surfaces", Report SU-SEL-64-025, Stanford Electronics Laboratories, Stanford University, Stanford, CA (April 1964).

Hagfors, T., "A Study of the Depolarization of Lunar Radar Echoes", Radio Sci., Vol. 2, p. 445 (1967).

Hey, J.S., and S.J. Parsons, "The Radar Measurement of Low Angles of Elevation", Phys. Soc. Proc., Vol. 69B, pp. 321-328 (October 1955).

Howard, D.D., et al, "Monopause Tracking Errors Due to Multipath: Causes and Remedies", in IEEE 1971 EASCON Rec., pp. 175-82 (1971).

Hundley, R.O., "Strategic Technology Final Report--Period 5 1974-30 June 1975", July 1975 (SECRET), R & D Associates, Santa Monica, CA, RDA-TR-4600-018.

Howard, E.E., S.M. Sherman, and D.N. Thompson, "Experimental Results of the Complex Indicated Angle Techniques for Elevation Measurement in the Multipath Region", presented at the 19th Tri-Service Radar Symposium, July 1973 (UNCLASSIFIED but not generally available).

Jasik, H. (ed.), Antenna Engineering Handbook, McGraw-Hill Book Co., New York, NY (1961).

Kerr, D.E., W.T. Fishback, and H. Goldstein, "Reflections from the Earth's Surface", in Propagation of Short Radio Waves, (D.E. Kerr, ed.), McGraw-Hill Book Co., New York, NY (1951).

Kodis, R.D., "A Note on the Theory of Scattering from an Irregular Surface", IEEE Proc. on Antennas and Propagation, Vol. AP-14, p. 77 (1966).

Kraus, J.D., Radioastronomy, McGraw-Hill Book Co., New York, NY (1969).

Ksienski, A., and R.B. McGhee, "A Decision Theoretic Approach to the Angular Resolution and Parameter Estimation Problem for Multiple Targets", IEEE Trans. on Aerosp. Electron. Syst., Vol. AES-4, pp. 443-445 (May 1968).

McGavin, R.E., and L.J. Maloney, "Study at 1046 Mc. of the Reflection Coefficient of Irregular Terrain at Grazing Angles", J. Res. Nat. Bur. Stand., Vol. 63D, p. 235 (1959).

Peake, W.H., "The Interaction of Electromagnetic Waves with Some Natural Surfaces", Report 898-2, Antenna Lab., Ohio State University, Columbus, OH (1959a).

Peake, W.H., "Theory of Radar Return from Terrain", IRE Interrat. Conv. Record, Vol. 7, Part 1:27 (1959b).

Peebles, P.Z., Jr., "Further Results on Multipath Angle Error Radiation Using Multiple-Target Methods", IEEE Trans. Aerosp. Electron. Syst., Vol. AES-9, p. 654 (1973).

Peebles, P.Z., Jr., and R. S. Berkowitz, "Multiple-Target Monopulse Radar Processing Techniques", IEEE Trans. Aerosp. Electron. Syst., Vol. AES-4, pp. 845-854 (1968).

Peebles, P.Z., Jr., and L. Goldman, Jr., "Radar Performance with Multipath Using the Complex Angle", IEEE Trans. Aerosp. Electron. Syst., Vol. AES-7, pp. 171-178 (1971).

Pollon, G.E., "On the Angular Resolution of Multiple Targets", IEEE Trans. Aerosp. Electron. Syst. (Corresp.), Vol. AES-3, pp. 145-148 (1967).

Pollon, G.E., and G. W. Lank, "Angular Tracking of Two Closely Spaced Radar Targets", IEEE Trans. Aerosp. Electron. Syst., Vol. AES-4, pp. 541-550 (1968).

Ramo, S., J. Whinnery, and T. Van Duzen, Fields and Waves in Communication Electronics, John Wiley & Sons, New York, NY (1966).

Rice, S.W., "Reflection of Electromagnetic Waves from Slightly Rough Surfaces", Communications on Pure and Applied Mathematics, pp. 351-378 (August, 1951).

Ruze, J., "Physical Limitations on Antennas", Massachusetts Institute of Technology Research Laboratory, Electron. Tech. Rept. 248, October 30, 1952.

Schwartz, M., and L. Shaw, Signal Processing, McGraw-Hill Book Co., New York, NY (1975).

Sherman, S.M., "Complex Indicated Angles Applied to Unresolved Radar Targets and Multipath", IEEE Trans. Aerosp. Electron. Syst., Vol. AES-7, pp. 160-170 (1971).

Sherman, S.M., "The Use of Complex Indicated Angles in Monopulse Radar to Locate Unresolved Targets", Proc. Natl. Electron. Conf., Vol. 22 (1966).

Simpson, R.A., "Lunar Radar Echoes: An Interpretation Emphasizing Characteristics of the Leading Edge", SEL Report SEL-73-027, Stanford Electronics Laboratories, Stanford University, Stanford, CA (1973).

Sklar, J.R., and F. C. Schwepps, "On the Angular Resolution of Multiple Targets", Proc. IEEE (Corresp.), Vol. 52, pp. 1044-1045 (September 1964).

Skolnik, M., ed., Radar Handbook, McGraw-Hill Book Co., New York, NY (1970).

Smith, B.G., "Geometrical Shadowing of a Random Rough Surface", IEEE Trans. on Antennas and Propagation, Vol. AP-15, p. 668 (1967).

Smith, P.G., and W.P. Melling, "Multipath Propagation Study", Report of General Research Corporation, Santa Barbara, CA (8 March 1974).

Symonds, M.D., and J.M. Smith, "Multifrequency Complex-Angle Tracking on Low-Level Targets", Radar Present and Future, IEEE Conf. Publ. No. 105, London, England, pp. 166-171 (October 23-25, 1973).

Tyler, G.L., and D.H.H. Ingalls, "Functional Dependencies of Bistatic-Radar Frequency Spectra and Cross Sections on Surface Scattering Laws", J. Geophys. Res., Vol. 76, p. 4774 (1971).

Tyler, G.L., and R.A. Simpson, "Bistatic Radar Measurements of Topographic Variations in Lunar Surface Slopes with Explorer 35", Radio Sci., Vol. 5, p. 263 (February 1970).

Tyler, G.L., R.A. Simpson, and H.J. Moore, "Lunar Slope Distributions: Comparison of Bistatic-Radar and Photographic Results", J. Geophys. Res., Vol. 76, p. 2790 (1971).

Tyler, G.L., and T. Howard, "Dual-Frequency Bistatic-Radar Investigations of the Moon with Apollos 14 and 15", J. Geophys. Res., Vol. 78, p. 4852 (1973).

Van De Pol, L., and M. Bremmer, "Further Note on the Propagation of Radio Waves over a Finitely Conducting Spherical Earth", Phil. Mag., Vol. 27, Series 7, No. 182 (1939).

Von Deusan, R., and W. Steckenreitar, AIL Report No. 5609-1, Cutler-Hammer Airborne Instrument Laboratory, Long Island, NY (1973).

Von Schlachta, K., "The Use of Target and Clutter Data for Different Methods of Discrimination Between Targets and Unwanted Clutter", Preprint of a paper written at Forschungsinstitut für Funk and Mathematik D-5307 Waehtberg-Werthoven, Germany (1973).

White, W.D., "Techniques for Tracking Low-Angle Radar Targets in the Presence of Multipath", IEEE Trans. Aerosp. Electron. Syst., Vol. AES-10, pp. 835-854 (1974).

DISTRIBUTION

Defense Advanced Research Projects Agency
1400 Wilson Blvd.
Arlington, VA 22209
ATTN: G. H. Heilmeier
D. J. Looft
R. F. Hoglund
R. A. Moore
S. Zakanycz
D. W. Walsh
C. W. Hartsell, Jr.
E. T. Gerry
LTC C. A. Osinski
CPT J. W. Justice
D. L. Anderson
E. H. Kopf
LTC W. Whitaker (2)

Institute for Defense Analysis
400 Army-Navy Drive
Arlington, VA 22209
ATTN: J. Bengston
H. Wolfhard

Naval Research Laboratory
4555 Overlook Ave., SW
Washington, DC 20390
ATTN: M. I. Skolnik, Code 5300
D. D. Howard
J. W. Wright
L. V. Blake

Ballistic Research Lab/Cal
Aberdeen Proving Grounds, MD 21005
ATTN: P. Dietz

Armament and Technology
Procurement Group
Berne, Switzerland
ATTN: T. P. Vasserot

ODDR&E
The Pentagon
Washington, DC 20301
ATTN: W. T. Delaney, Rm. 3D136

BGEN J. A. Welch, Jr.
Hdqs., USAF/AFXO
The Pentagon, Rm 4D1069
Washington, DC 20330

General Research Corp.
P.O. Box 3587
Santa Barbara, CA 93105
ATTN: J. Cunningham
A. V. Mrstik
P. G. Smith
W. P. Melling
G. VanBlaricum

Raytheon Co.
Wayland, MA 01778
ATTN: D. Barton
D. G. Armstrong
P. E. Cornwell
A. H. Greene

Airborne Instruments Laboratory
A Division of Cutler-Hammer, Inc.
Camac Rd.
Deer Park, NY 11729
ATTN: W. D. White
R. Van Deusan
W. Steckenreiter

Dr. D. E. Barrick
NOAA
Boulder, CO 80302

Dr. Peter Beckmann (2)
Physics Department
The University of Colorado
Boulder, CO 80302

Lockheed Palo Alto Research Laboratory
Hanover St.
Palo Alto, CA 94304
ATTN: W. McCormac
F. H. Maltz

Dr. W. C. Meecham
UCLA
405 Hilgard Ave.
Los Angeles, CA 90024

Dr. R. Stewart
IGPP
Scripps Institution of Oceanography
University of California
La Jolla, CA 92037

Illinois Institute of Technology
Department of Electrical Engineering
Chicago, IL 60616
ATTN: S. R. Borkar
R. F. H. Yang

Stanford Center for Radar Astronomy
Durand 229
Stanford, CA 94305
ATTN: G. L. Tyler
V. R. Eshleman
H. T. Howard
A. M. Despain

Royal Radar Establishment
St. Andrews Road
Malvern, Worcestershire
ENGLAND
ATTN: J. R. Shayler, Deputy Director
A. K. Edgar

Jet Propulsion Laboratory
California Institute of Technology
1800 Oak Grove Dr.
Pasadena, CA 91103
ATTN: J. Dunne, 180-401
C. Elachi, 183-701

Center for Research, Inc.
University of Kansas
Lawrence, KS 66044
ATTN: R. K. Moore
A. K. Fung
A. Leovaris

CALSPAN Corp.
4455 Genesee St.
Buffalo, NY 14221
ATTN: T. R. Benedict
R. E. Kell

MIT Lincoln Laboratory
P.O. Box 73
Lexington, MA 02173
ATTN: R. D. Kodis
R. A. Brocklemann
Report Librarian

USGS
Astrogeological Studies
345 Middlefield Rd.
Menlo Park, CA 94025
ATTN: R. J. Pike

Battelle Memorial Institute
505 King Ave.
Columbus, OH 43201
ATTN: G. T. Ruck
W. D. Stuart
C. K. Krichbaum
STOICA
TACTEC

Dr. David L. Book, Code 7750
Head, Theoretical Section
Plasma Dynamics Branch
Naval Research Laboratory
Washington, DC 20375

RCA
Missile & Surface Radar Div.
Marne Hwy.
Moorestown, NJ 08057
ATTN: J. T. Nessmith
S. M. Sherman

Ferranti Ltd.
Wythenshawe
Manchester 22, ENGLAND
ATTN: G. C. Evans

Dr. Karl von Schlachta
Forschungsinstitut für Funk und Mathematik
D-5307 Wachtberg-Werthoven
GERMANY

Bellcomm, Inc.
Washington, DC 20036
ATTN: B. G. Smith

Engineering Experiment Station
Georgia Institute of Technology
Atlanta, GA 30332
ATTN: H. A. Corriher
B. O. Pyron

Dr. R. R. Goodman Code 8000
Associate Director of Research
Naval Research Laboratory
Department of the Navy
Washington, DC 20375

R&D Associates
P.O. Box 9695
4640 Admiralty Way
Marine del Rey, CA 92091
ATTN: R. O. Rundley (2)

Stanford Research Institute
333 Ravenswood Ave.
Menlo Park, CA 94025
ATTN: P. H. Bentley
D. A. Johnson
J. C. Schlobohm
W. E. Jaye
A. A. Burns
J. D. Pressnell
N. Cianos
A. M. Peterson

Dr. J. F. Vesecky
Astronomy Department
The University
Leicester LE1 7RH, ENGLAND

Dr. F. W. Perkins, Jr.
Plasma Physics Laboratory
Princeton University
Princeton, NJ 08540

Dr. R. A. Muller
2831 Garber St.
Berkeley, CA 94705

RADC (OCSE)
Griffiss AFB, NY 31411
ATTN: R. Urtz (2)

Hughes Research Laboratories
3011 Malibu Canyon Road
Malibu, CA 90265
ATTN: J. Jenney

Ohio State University
Antenna Laboratory
1320 Kinnear Road
Columbus OH 43212
ATTN: Report Librarian

Defense Documentation Center (12)
Cameron Station
Alexandria, VA 22314